AD-A158 697 PAPST (PLASTIC AXISYMMETRIC/PLANAR STRUCTURES) - REVISION 20 REVISED DOCU..(U) LITTLE (ARTHUR D) INC CAMBRIDGE MA P D HILTON ET AL. AUG 82 ADL-87058 1/1

UNCLASSIFIED N00167-81-C-0260 F/G 9/2 NL

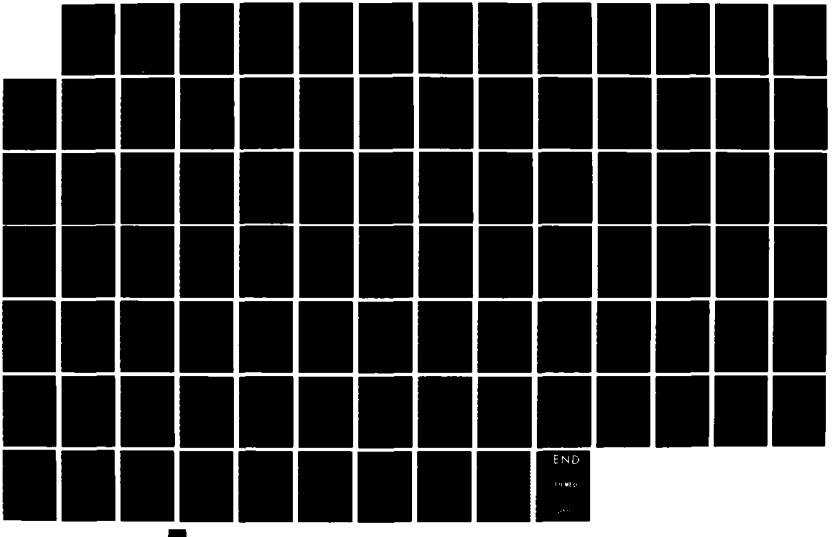

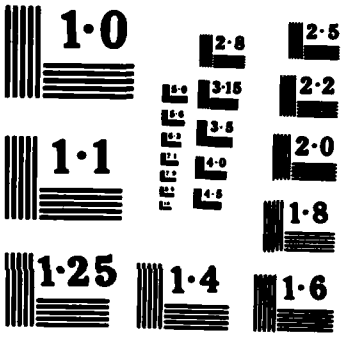

PAPST - REVISION 2.0
REVISED DOCUMENTATION
AND
THEORETICAL MANUAL

REPORT TO

DAVID TAYLOR NAVAL SHIP R&D CENTER
BETHESDA, MARYLAND 20084

AUGUST 1982

CONTRACT N00167-81-C-0260

CASE NO. 87058

BY

PETER D. HILTON
D. DOUGLAS WILMARTH

Arthur D. Little, Inc.

ACKNOWLEDGEMENTS

The authors would like to thank Dr. Ron Mayville and Ms. Barbara Forman for their help in developing the theory and the computer program described in this report, and Ms. Donna Canty for the report preparation. Special thanks goes to Mr. L. Nash Gifford at DTNSRDC for his continuing support of our development efforts.

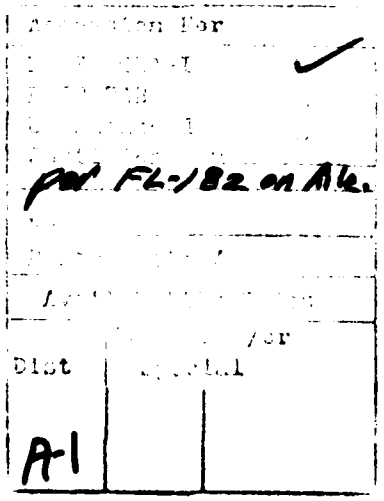

TABLE OF CONTENTS

LIST OF FIGURES

LIST OF TABLES

1.0 INTRODUCTION

The computer program PAPST, standing for Plastic Axisymmetric/Planar STructures (Reference 1), has been developed with the Navy with the aim of addressing the elastic-plastic crack problems which arise from material and structural considerations associated with the use of high toughness materials. Both power hardening and multilinear models for uniaxial stress-strain response are available. Enriched elements may be used to model the material crack tip response for the multilinear material model. For crack problems, both path values for the J integral and values based on the amplitude of the singular solution can be computed.

The program has been used in support of laboratory programs to develop material property data for J_{Ic} and other pertinent parameters for fracture characterization. More recently, the capabilities of PAPST have been extended to include simulation of quasi-static crack growth. This procedure is of interest in determination of the Tearing Modulus (Reference 2) and in assessing the stability of crack growth.

Incorporated into PAPST is its predecessor APES, standing for Axisymmetric/Planar Elastic Structures (References 3,4). Also developed with the Navy, APES performs linear elastic fracture mechanics for Mode I and Mode II problems. It has the capability to handle crack face loadings and a limited capability to deal with orthotropic materials.

Additional layers of [illegible];
Coordinate Specifications, (

2.0 PROGRAM DESCRIPTION

This report is to review and update the theoretical basis and present capabilities of the computer program PAPST. This program, and its predecessor APES, have been in development for ten years by the Navy. The present revision of PAPST has involved a major restructuring of the basic computer code to facilitate future development. Several options that were in previous revisions have been dropped because they proved to be inaccurate. Many of the important capabilities have been rederived to be internally consistent. New features have been added to enhance the program. The modifications are extensive, requiring a complete review of the program.

Present capabilities include:

1) Elastic orthotropic material properties.

2) Elastic/perfectly plastic, power hardening, and multilinear isotropic models for elastic/plastic material behavior.

3) Cubic isoparametric plane elements with three (9-node) or four (12-node) sides, with optional enrichment to accommodate the crack tip asymptotic solution.

4) Concentrated and distributed elastic springs.

5) Tied nodal displacements.

6) Concentrated and distributed tractions.

7) Crack face pressure loading.

8) Thermal loading.

9) Mode I and II elastic stress intensity factors.

10) Mode I plastic stress intensity factors.

11) J-integral calculation from stress intensity factors and from path integrals.

12) Finite strain treatment.

13) Load, displacement or thermal controlled incremental loading.

14) Wavefront reordering.

15) Plotting of displacements, stress contours and thermal contours.

Both enriched and regular models can be analyzed using the non-linear stress-strain relationships detailed in Section 2.1. The program will automatically scale the elastic solution to yielding of the highest stressed quadrature point. Subsequent increments are either defined by the user or evenly stepped to full loading. Inclusion of the large deformation calculation is optional. The degree of accuracy can also be user supplied.

2.0.1 Plasticity Theory

PAPST incorporates incremental J_2-flow theory plasticity (von Mises yield criterion). The components of the deviatoric strain rate are expressed in terms of the current deviatoric stress components and the components of the deviatoric stress rate as

$$\dot{e}_{ij} = \begin{cases} \frac{1+\nu}{E}\dot{S}_{ij} + \frac{3}{2} f(\sigma_e) S'_{ij} \dot{\sigma}_e & \left[\sigma'_e = \sigma_{yd},\ \dot{\sigma}_e > 0\right] \\ \frac{1+\nu}{E}\dot{S}_{ij} & \text{(otherwise)} \end{cases} \qquad (2.0.1\text{-}1)$$

where e_{ij} are the deviatoric strain rate components

$$\dot{e}_{ij} = \dot{\varepsilon}_{ij} - \frac{1}{3}\dot{\varepsilon}_{pp}\delta_{ij} \qquad (2.0.1\text{-}2)$$

S_{ij} are the current deviatoric stress components

$$S_{ij} = \sigma_{ij} - \frac{1}{3}\sigma_{pp}\delta_{ij} \qquad (2.0.1\text{-}3)$$

S'_{ij} are the deviatoric stress components measured from the center of the current yield surface

$$S'_{ij} = S_{ij} - a_{ij} \qquad (2.0.1\text{-}4)$$

a_{ij} are the coordinates in stress space of the center of the yield surface, σ_e is the von Mises effective stress

$$\sigma_e = \sqrt{\frac{3}{2} S_{ij}S_{ij}} \qquad (2.0.1\text{-}5)$$

and σ'_e is the effective stress as measured from the center of the yield surface and σ_{yd} is the yield stress.

$$\sigma'_e = \sqrt{\frac{3}{2} S'_{ij} S'_{ij}} \qquad (2.0.1\text{-}6)$$

The function $f(\sigma_e)$ in Equation 2.0.1-1 is derived from a uniaxial stress-strain curve as described subsequently (Reference 5)

The hydrostatic strain rate is given in terms of the mean stress rate as

$$\dot{\varepsilon}_{pp} = \frac{1-2\nu}{E} \dot{\sigma}_{pp} \qquad (2.0.1\text{-}7)$$

The center of the yield surface can move under plastic deformation at a rate proportional to the projection of the stress rate vector onto the local normal to the yield surface. The motion of the yield surface center is directed along the vector describing the deviatoric stress relative to the yield surface center,

$$\dot{a}_{ij} = \begin{cases} \frac{3}{2} \beta S'_{kl} \dot{S}_{kl} S'_{ij} / (\sigma'_e)^2 & \left[\sigma'_e = \sigma_{yd} \right. \\ & \left. \dot{\sigma}_\epsilon > 0 \right] \\ 0 \quad \text{[otherwise]} & \\ 0 \leq \beta \leq 1 & \end{cases} \qquad (2.0.1\text{-}8)$$

where β is to be specified by the program user. Isotropic hardening is achieved by setting β equal to zero and kinematic hardening results when β is set equal to one. Intermediate cases between these two extremes may be achieved. These possibilities are indicated in Figure 2.0.1-1 which shows various yield surfaces on the π plane in stress space, and corresponding examples of uniaxial bilinear stress strain curves obtained with each hardening model. For uniaxial or proportional states of stress, all hardening models would give the same result provided there is no reversed yielding. For multi-axial states of stress, on the other hand, the kinematic and isotropic hardening models can give significantly different results if the loading is strongly non-proportional and/or if reverse yielding occurs.

2.0.2 Finite Strain Treatment

PAPST incorporates finite strain effects through the use of an updated Lagrangian formulation (Reference 6), i.e., the coordinate system is convected with the deformation. In this coordinate system the relationship between true strain rate and the deformation rate (or velocity) is unchanged from the small strain theory equations. Also the true (or Cauchy) stress rate tensor relates to the true strain rate in the classical sense,

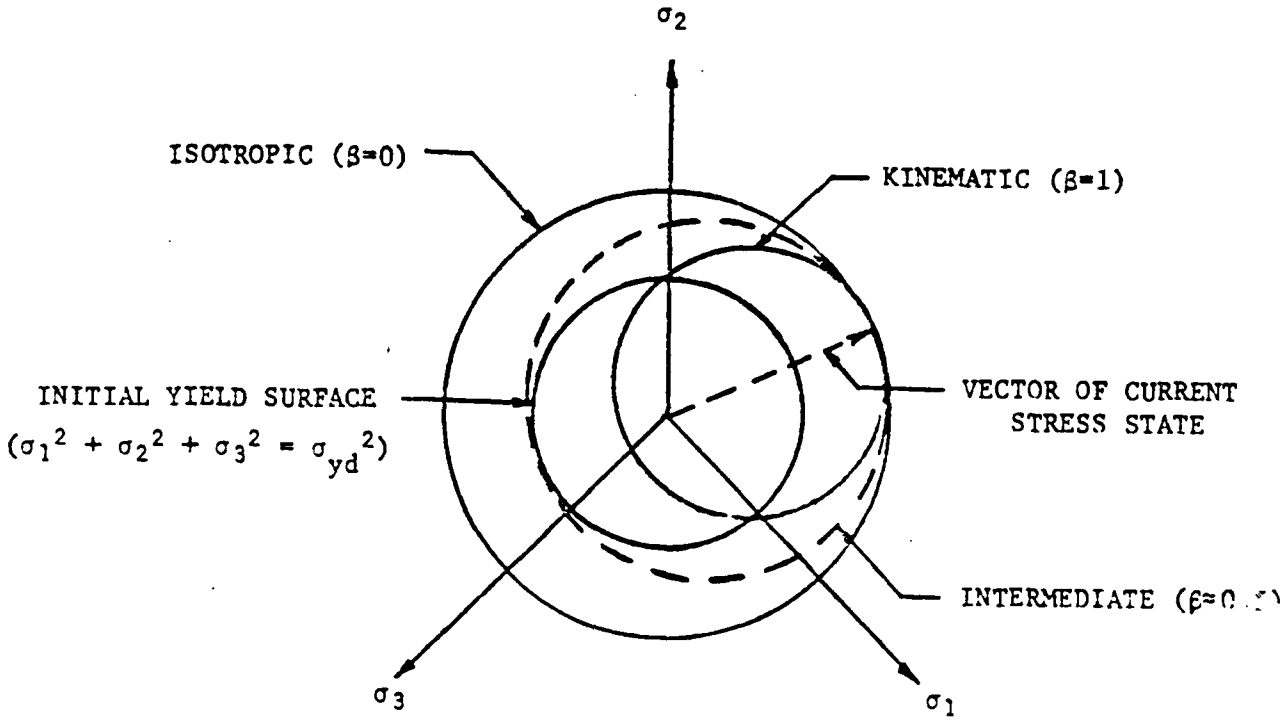

π Plane Comparison of Subsequent Yield Surfaces for Various Hardening Rules

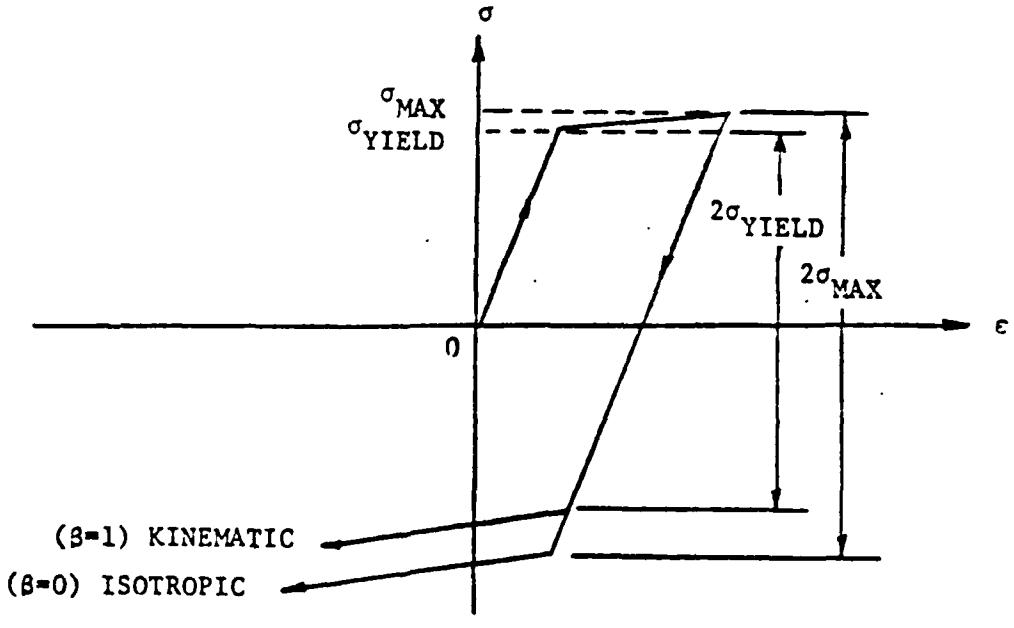

Uniaxial Bilinear Stress-Strain Curves for Kinematic and Isotropic Hardening Models

Figure 2.0.1-1 Diagrams of Isotropic and Kinematic Hardening Models

$$\dot{\sigma}^{c}_{ij} = C_{ijkl}\,\dot{\epsilon}_{kl} \qquad (2.0.2\text{-}1)$$

where the subscripts take values of one to three and repeated subscripts imply summation.

The Cauchy stress tensor is not invariant under finite rotations, but rather at zero strain rate it changes at the rate (Reference 31).

$$\dot{\sigma}^{c}_{ij} = \dot{W}_{ip}\sigma^{c}_{pj} - \dot{W}_{pj}\,\sigma^{c}_{ip} \qquad (2.0.2\text{-}2)$$

where $\dot{W}_{ij}$ is the rotation rate tensor. Equations 2.0.2-1 and 2.0.2-2 are combined to express the Cauchy stress rate in terms of the true strain and rotation rates as

$$\dot{\sigma}^{c}_{ij} = C_{ijkl}\dot{\epsilon}_{kl} + \dot{W}_{ik}\sigma^{c}_{kj} - \dot{W}_{kj}\,\sigma^{c}_{ik} \qquad (2.0.2\text{-}3)$$

2.0.3 Iterative Solution Procedure

The governing matrix equation for finite elements is

$$K\,U = P \qquad (2.0.3\text{-}1)$$

Where: K is the stiffness matrix

U is the displacement vector

P is the load vector

For elastic solutions, the stiffness matrix is constant, and the solution can be determined explicitly. Incremental plasticity implies that the stiffness matrix is a function of the displacement vector. Because of this, the stiffness matrix can only be determined instantaneously. This requires that the loading be incremental and that the solution must be iterated until the instantaneous stiffness matrix and the incremental displacements agree with the applied loading increment,i.e.,

$$K(u)\,\Delta U = \Delta P \qquad (2.0.3\text{-}2)$$

The formulation of the instantaneous stiffness matrix is:

$$\dot{K}(u) = \sum_{\text{elements}} \int_{\text{area}} B^T(u)\, C(u)\, B(u)\, dA \qquad (2.0.3\text{-}3)$$

Equation 2.0.3-2 is solved for the estimate of ΔU by using the previous U vector to calculate $K(u)$.

The load correction vector is then determined as

$$\sum_{\text{increments}} \Delta P \; - \sum_{\text{increments}} K(u)\, \Delta U = \Delta\Delta P \qquad (2.0.3\text{-}4)$$

and the equation

$$K(u)\Delta\Delta U = \Delta\Delta P \qquad (2.0.3\text{-}5)$$

is solved to obtain the correction to ΔU.

However, it is not necessary to perform the complete computation implied in Equation 2.0.3-3 to obtain the load correction vector, rather

$$\begin{aligned} K(u)\,\Delta U &= \sum_{\text{elements}} \int_{\text{area}} B^T(u)\, C\,(u)\, B(u)\, dA\, \Delta U \\ &= \sum_{\text{elements}} \int_{\text{area}} B^T(u)\, C(u)\, \Delta\varepsilon dA \\ &= \sum_{\text{elements}} \int_{\text{area}} B^T(u)\Delta\sigma\, dA \end{aligned} \qquad (2.0.3\text{-}6)$$

An exception to this procedure should be made for any elements for which the stiffness matrix is readily available. This is the case for both concentrated and distributed springs since they are elastic, i.e.,

$$K(u)\,\Delta U = \sum_{\text{elements}} \int_{\text{area}} B^T(u)\,\Delta\sigma\,dA + \sum_{\text{springs}} K_{sp}\,\Delta U \qquad (2.0.3\text{-}7)$$

Two different convergence criteria have been set-up:

$$[|\Delta\Delta P| / |P|]^{1/2} \leq \text{conv}_1 \qquad (2.0.3\text{-}8)$$

for overall convergence, and

$$[|\Delta\Delta P| / |\Delta P|]^{1/2} \leq \text{conv}_2 \qquad (2.0.3\text{-}9)$$

for increment convergence. Both must be satisfied in PAPST at each increment.

2.0.4 Yield Surface Modification

Once an increment has converged, the yield surfaces of each node and quadrature point are modified to reflect the new stress state. The new coordinates of the center of the yield surface are:

$$a'_{ij} = a_{ij} + \beta[\sigma'_e - r]\, S'_{ij}/\sigma'_e \qquad (2.0.4\text{-}1)$$

where r = radius of the previous yield surface

$$r' = r + (1-\beta)\,(\sigma'_e - r) \qquad (2.0.4\text{-}2)$$

The yield surface is modified when the increment calculation has converged.

2.1 Material Models

The material model describes the relationship of the stress vector to the strain vector:

$$\underset{\sim}{\sigma} = C \underset{\sim}{\varepsilon} \tag{2.1-1}$$

$$\underset{\sim}{\varepsilon} = C^{-1} \underset{\sim}{\sigma} = D \underset{\sim}{\sigma} \tag{2.1-2}$$

$\underset{\sim}{\sigma}$ is the stress vector

$\underset{\sim}{\varepsilon}$ is the strain vector

Where C and D are the constitutive material matrices

The material matrices in the elastic range are constant and may be specified with direction dependent (orthotropic) properties. In the plastic analysis, the matrices are restricted to isotropic properties but may describe a non-linear stress-strain relationship. The material matrices will then reflect the instantaneous relationship. Options are available for either power hardening or multilinear material models. Either of these models can be used to approximate a true stress/true strain curve that has been experimentally derived.

2.1.1 Orthotropic Elastic Model

The orthotropic stress-strain relation for an axisymmetric element is:

$$\begin{bmatrix} \varepsilon_x \\ \varepsilon_y \\ \varepsilon_z \\ \gamma_{xy} \end{bmatrix} = \begin{bmatrix} 1/E_x & -\nu_{yx}/E_y & -\nu_{zx}/E_z & 0 \\ -\nu_{xy}/E_x & 1/E_y & -\nu_{zy}/E_z & 0 \\ -\nu_{xz}/E_x & -\nu_{yz}/E_y & 1/E_z & 0 \\ 0 & 0 & 0 & 1/G_{xy} \end{bmatrix} \begin{bmatrix} \sigma_x \\ \sigma_y \\ \sigma_z \\ \tau_{xy} \end{bmatrix} \tag{2.1.1-1}$$

The ten independent variables reduce to seven if we impose the Maxwell's reciprocal relations:

$$\frac{E_x}{\nu_{xy}} = \frac{E_y}{\nu_{yx}} ; \frac{E_y}{\nu_{yz}} = \frac{E_z}{\nu_{zy}} ; \frac{E_x}{\nu_{xz}} = \frac{E_z}{\nu_{zx}} \qquad (2.1.1\text{-}2)$$

Isotropic properties are a special case in that there are only two independent parameters:

Poisson's Ratio $\nu = \nu_{xy} = \nu_{yz} = \nu_{zx}$ (2.1.1-3)

Young's Modulus $E = E_x = E_y = E_z$ (2.1.1-4)

with

$$G = G_{xy} = E/2(1 + \nu) \qquad (2.1.1\text{-}5)$$

For plane strain, the constraint exists that the out-of-plane strain must be zero:

$$\varepsilon_z = 0 \qquad (2.1.1\text{-}6)$$

For this case the C matrix remains unchanged, but the D matrix becomes:

$$\begin{bmatrix} D_{11} - \frac{D_{13}D_{31}}{D_{33}} & D_{12} - \frac{D_{13}D_{32}}{D_{33}} & 0 & D_{14} - \frac{D_{13}D_{34}}{D_{33}} \\ & D_{22} - \frac{D_{23}D_{32}}{D_{33}} & 0 & D_{24} - \frac{D_{23}D_{34}}{D_{33}} \\ & & 0 & 0 \\ [SYM] & & & D_{44} - \frac{D_{43}D_{34}}{D_{33}} \end{bmatrix} \qquad (2.1.1\text{-}7)$$

For plane stress the constraint is on the out-of-plane stress:

$$\sigma_z = 0 \qquad (2.1.1\text{-}8)$$

The D matrix remains unchanged, but the C matrix is modified similarly to the D matrix in plane strain.

$$\begin{bmatrix} C_{11} - \frac{C_{13}C_{31}}{C_{33}} & C_{12} - \frac{C_{13}C_{32}}{C_{33}} & 0 & C_{14} - \frac{C_{13}C_{34}}{C_{33}} \\ & C_{22} - \frac{C_{23}C_{32}}{C_{33}} & 0 & C_{24} - \frac{C_{23}C_{34}}{C_{33}} \\ & & 0 & 0 \\ [SYM] & & & C_{44} - \frac{C_{43}C_{34}}{C_{33}} \end{bmatrix} \qquad (2.1.1\text{-}9)$$

The program has fully implemented the use of the orthotropic relationship for elastic problems.

2.1.2 Elastic/Perfectly Plastic Model

For a uniaxial stress state the following relationship exists for this model:

$$\sigma = \begin{cases} \varepsilon E & \text{for} \quad \varepsilon < \sigma_{yd}/E \\ \sigma_{yd} & \text{for} \quad \varepsilon \geq \sigma_{yd}/E \end{cases} \qquad (2.1.2\text{-}1)$$

This relationship is useful in plasticity calculations only. It is not used in fracture mechanics or J-integral analyses. The application of this relationship is primarily for comparison of results to theoretical solutions for which it is analytically convenient to assume elastic/perfectly plastic behavior.

The power hardening and multilinear models can be specified such that they simulate elastic/perfectly plastic material response.

2.1.3 Power Hardening (Ramberg-Osgood) Model

In the case of the power hardening simulation of material response (Ramberg-Osgood), the uniaxial response is given as

$$\varepsilon = \begin{cases} \sigma/E & \text{for } \sigma \leq \sigma_{yd} \\ \sigma/E + \alpha\left[\frac{\sigma}{E}\left(\frac{\sigma}{\sigma_{yd}}\right)^{n-1} - \frac{\sigma_{yd}}{E}\right] & \text{for } \sigma > \sigma_{yd} \end{cases} \qquad (2.1.3\text{-}1)$$

The correlation parameters and the initial yield stress are chosen to best model the observed behavior. Note that if n = 1, A bilinear material model is achieved. In this case the strain hardening slope is given by:

$$\Delta\sigma/\Delta\varepsilon = E/(1+\alpha) \qquad (2.1.3\text{-}2)$$

For the power hardening material model, the plastic component of the strain is given by

$$\varepsilon_p = \frac{\alpha\sigma^n}{E\sigma_{yd}^{n-1}} - \frac{\alpha\sigma_{yd}}{E} \qquad (2.1.3\text{-}3)$$

and the plastic strain rate is thus

$$\dot{\varepsilon}_p = \frac{\alpha n\sigma^{n-1}\dot{\sigma}}{E\sigma_{yd}^{n-1}} \qquad (2.1\text{-}3\text{-}4)$$

The power hardening material model is illustrated in Figure 2.1-1. For this model, the function $f(\sigma_e)$ (Equation 2.Ø.1-1) which relates the plastic strain rate to plastic stress rate is

$$f(\sigma_e) = \frac{\alpha n}{E\sigma_{yd}}\left[\frac{\sigma_e}{\sigma_{yd}}\right]^{n-2} \qquad (2.1.3\text{-}5)$$

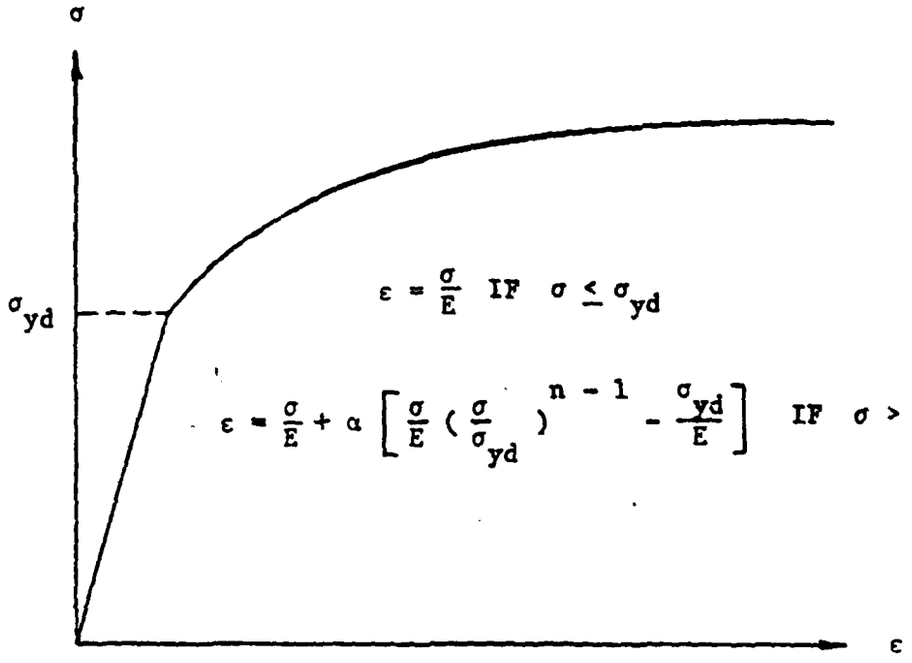

Power Hardening Material Model

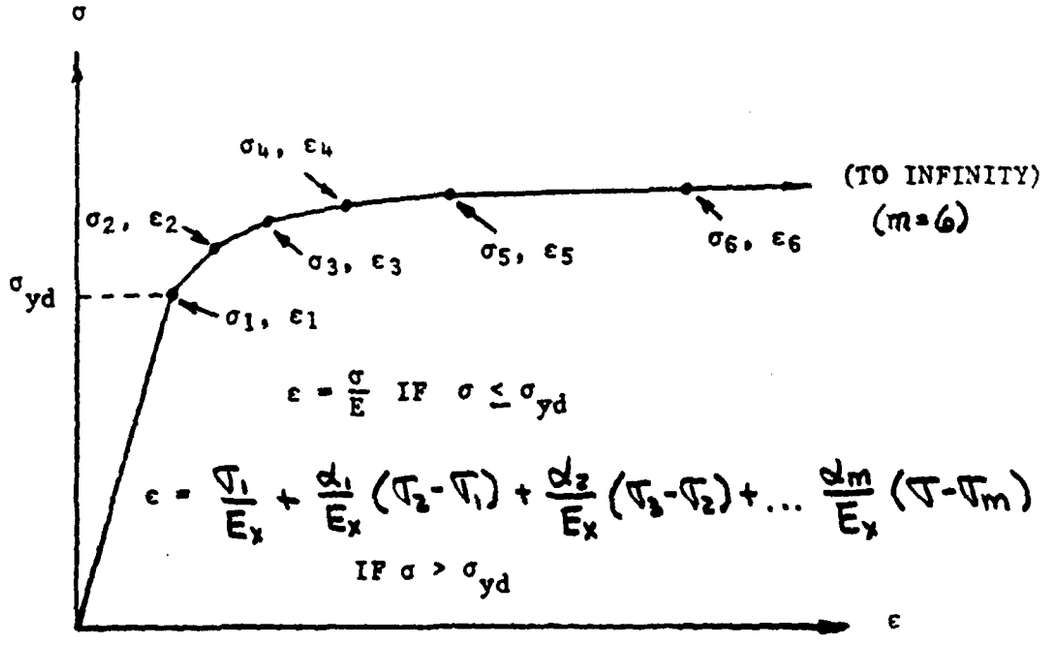

Multilinear Material Model

Figure 2.1-1 Available True Stress - True Strain Models

2.1.4 Multilinear Model

The mathematical form for the multilinear model of material behavior is

$$\varepsilon = \frac{\sigma}{E} + \frac{\alpha_1}{E}(\sigma_2 - \sigma_1) + \frac{\alpha_2}{E}(\sigma_3 - \sigma_2) + \ldots \frac{\alpha_m}{E}(\sigma - \sigma_m) \qquad (2.1.4\text{-}1)$$

$$\sigma_m < \sigma \leq \sigma_{m+1} \qquad (2.1.4\text{-}2)$$

For this material model, the plastic strain rate is given by

$$\dot{\varepsilon}_p = \alpha_m \dot{\sigma}_e / E \qquad (2.1.4\text{-}3)$$

and

$$f(\sigma_e) = \alpha_m / E\sigma_e \qquad (2.1.4\text{-}4)$$

The multilinear material model divides the uniaxial response into one elastic and m-1 plastic straight line segments, where -m is used as data input to indicate the number of stress-strain pairs or "breakpoints" needed to define the multilinear model. The user then specifies the true stress and true strain at yield and (m-1) other points on the response curve. The last (mth) segment continues at constant slope to infinite strain regardless of the strain level actually used to define the slope of this segment. An example of this model is shown in Figure 2.1-1.

2.2 Elements

The element library of PAPST contains six elements:

1) 12-node isoparametric quadrilateral
2) 12-node enriched quadrilateral
3) 9-node isoparametric triangle
4) 9-node enriched triangle
5) 2-node concentrated spring
6) 8-node distributed spring

Except for the concentrated spring, the element stiffness matrix formulation is based on the Gaussian quadrature integration described in Zienkiewicz (Chapter 8, Reference 7). The concentrated spring stiffness matrix can be defined explicitly so that integration is not necessary.

The following discussion is provided so that the user can understand the basic theory and so that the notation can be defined.

Isoparametric elements are defined as elements in which the functions used to describe the geometry and the displacements are the same. Depending on the element, these shape functions can describe a line, an area, or a volume. Using these functions, we can map a distorted shape in physical coordinates to a simple shape in local or mapped coordinates. The stiffness matrix of the simple shape can be found generically and used for a larger class of physical element shapes. For example, the 12-node element is applicable to rectangles, trapezoids, parallelograms, four-sided circular sectors, and so on for any element with four sides in which each side can be described adequately by a cubic function.

For purposes of this discussion, we will use shape functions that define an area element. The shape is restricted to the X-Y physical cooodinate system. In mapped space, this translates to the s-t local coordinate system. The shape functions will be polynominal in the s-t coordinate system.

The geometry can be described at a point by the shape functions evaluated in the mapped space multiplied by the nodal values of the global coordinates. (Note: there are as many shape functions as nodes.)

$$X = \sum_{i=1}^{n} N_i(s,t)X_i \quad ; \quad Y = \sum_{i=1}^{n} N_i(s,t)Y_i \qquad (2.2\text{-}1)$$

where: N_i are the shape functions
X_i and Y_i are the nodal global coordinates

Similarly, the displacements at these nodes are described:

$$U = \sum_{i=1}^{n} N_i(s,t)U_i \; ; \; V = \sum_{i=1}^{n} N_i(s,t)V_i \qquad (2.2\text{-}2)$$

where U_i and V_i are the nodal global displacements (U corresponds to X and V to Y).

The strains within the area can be found by using the appropriate derivatives of the shape functions:

$$\epsilon = B\delta = \sum_{i=1}^{n} B \begin{bmatrix} U_i \\ V_i \end{bmatrix} \qquad (2.2\text{-}3)$$

where: B is the matrix of shape function derivatives appropriate for the type of analysis. In plane stress or plane strain the following holds:

$$\begin{bmatrix} \varepsilon_x \\ \varepsilon_y \\ \gamma_{xy} \end{bmatrix} = \sum_{i=1}^{n} \begin{bmatrix} \frac{\partial N_i}{\partial x} & 0 \\ 0 & \frac{\partial N_i}{\partial y} \\ \frac{\partial N_i}{\partial y} & \frac{\partial N_i}{\partial x} \end{bmatrix} \begin{bmatrix} U_i \\ V_i \end{bmatrix} \qquad (2.2\text{-}4)$$

while in axisymmetric problems:

$$\begin{bmatrix} \varepsilon_r \\ \varepsilon_z \\ \varepsilon_\theta \\ \gamma_{rz} \end{bmatrix} = \sum_{i=1}^{n} \begin{bmatrix} \frac{\partial N_i}{\partial r} & 0 \\ 0 & \frac{\partial N_i}{\partial z} \\ \frac{1}{r}N_i & 0 \\ \frac{\partial N_i}{\partial z} & \frac{\partial N_i}{\partial r} \end{bmatrix} \begin{bmatrix} U_i \\ V_i \end{bmatrix} \qquad (2.2\text{-}5)$$

Note: in PAPST the axisymmetric coordinate system is: r, z, θ corresponding to (x, y, z). Also, for consistency all problems take the dimensions of Equation 2.2-5 and for plane problems the terms in B corresponding to ε_z are zero.

The element stiffness matrix is defined as

$$K = \int_{\text{area}} B^T C B = \int_{-1}^{1}\int_{-1}^{1} B^T C B \,|\det J|\, ds\, dt \qquad (2.2\text{-}6)$$

where C is defined in Equation 2.1-1 and det J is the determinate of the Jacobian of the coordinate transformation. The integration is performed using Gaussian quadrature as

$$K = \sum_i \sum_j B^T C B \,|\det J| \,\Big|_{s_i, t_j} W_i W_j \qquad (2.2\text{-}7)$$

where W_i is the weight function corresponding to the ith quadrature point.

2.2.1 12-Node Quadrilateral Element

The element is shown in both the global coordinate and its mapped coordinate systems in Figure 2.2.1-1. The edges of the element correspond to values of s or t of $\pm$ 1, and the midside nodes correspond to values of s or t of $\pm 1/3$.

The order of the element is cubic meaning that the geometry and displacement components can vary along the element edge as a third order polynomial. Strains given by the derivatives of the shape functions may vary quadratically over the element. The specific shape functions for this element are:

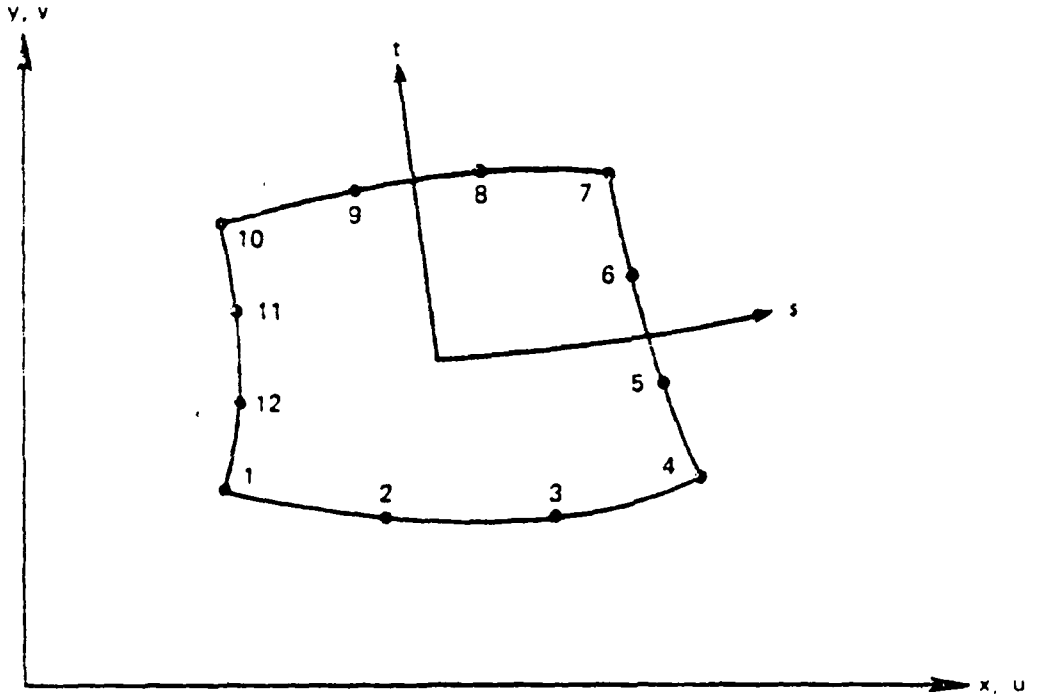

Global Coordinate System

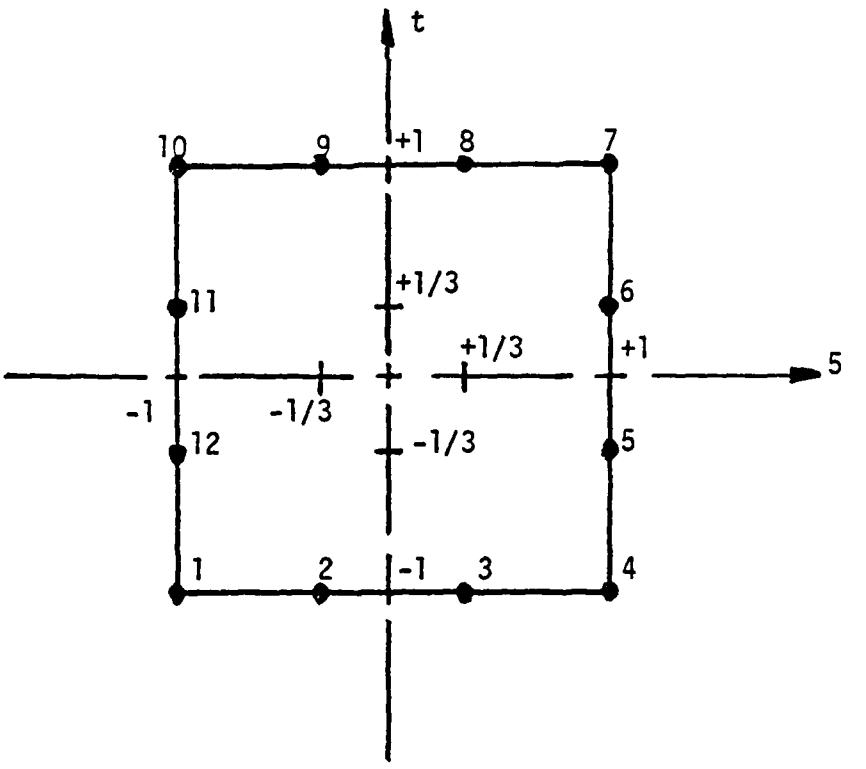

Mapped Coordinate System

Figure 2.2.1-1 12-Node Quadrilateral Element and Local Element Node Numbers

(2.2.1-1)

$$N_1 = \frac{1}{32}(1 - t)(1 - s)[-10 + 9(s^2 + t^2)]$$

$$N_2 = \frac{9}{32}(1 - t)(1 - s^2)(1 - 3s)$$

$$N_3 = \frac{9}{32}(1 - t)(1 - s^2)(1 + 3s)$$

$$N_4 = \frac{1}{32}(1 - t)(1 + s)[-10 + 9(s^2 + t^2)]$$

$$N_5 = \frac{9}{32}(1 + s)(1 - t^2)(1 - 3t)$$

$$N_6 = \frac{9}{32}(1 + s)(1 - t^2)(1 + 3t)$$

$$N_7 = \frac{1}{32}(1 + s)(1 + t)[-10 + 9(s^2 + t^2)]$$

$$N_8 = \frac{9}{32}(1 + t)(1 - s^2)(1 + 3s)$$

$$N_9 = \frac{9}{32}(1 + t)(1 - s^2)(1 - 3s)$$

$$N_{10} = \frac{1}{32}(1 + t)(1 - s)[-10 + 9(s^2 + t^2)]$$

$$N_{11} = \frac{9}{32}(1 - s)(1 - t^2)(1 + 3t)$$

$$N_{12} = \frac{9}{32}(1 - s)(1 - t^2)(1 - 3t)$$

The isoparametric elements can be "enriched" to account for the singularity at the tip of a crack as is discussed in Section 2.6.1.1. The 12-node enriched element involves the addition of another shape function, or creation of a sub-parametric element. The functions used to describe the geometry are the same as the isoparametric case, but the displacement field generated by the crack tip singularity is added to the displacements. Notation for this will be:

$$\epsilon^* = B^* \begin{bmatrix} K_I \text{ or } K_p \\ K_{II} \end{bmatrix} \quad \text{(if needed)} \tag{2.2.1-2}$$

where the definition of these fields are detailed in Section 2.6.1. These modifications to the shape functions are also reflected in the element stiffness matrix:

$$B' = B + B^* \tag{2.2.1-3}$$

$$K = \int_{\text{area}} (B')^T C B' \, d\Delta \tag{2.2.1-4}$$

2.2.2 9-Node Triangular Element

This element is developed as an extreme case of the 12-node quadrilateral element. The shape functions for the fourth side are combined into the first node. Gaussian quadrature is still used except that the accuracy is biased by the skewing of the integration toward the first corner of the element. When the element stresses are smoothed to the nodes, the same smoothing is applied as the quadrilateral except that the stresses for the fourth side are averaged at the first node.

Since we use the collapsed quadrilateral, no change in the enrichment procedure is required.

2.2.3 8-Node Distributed Spring

The 8-node distributed spring was developed to provide the same order of accuracy in elastic boundary conditions as is provided by the 12-node quadrilateral element. The stiffness matrix for the distributed spring is calculated using a modified line integral based on Gaussian quadrature. Inputs to the subroutine are the axial and shear stiffnesses of the spring

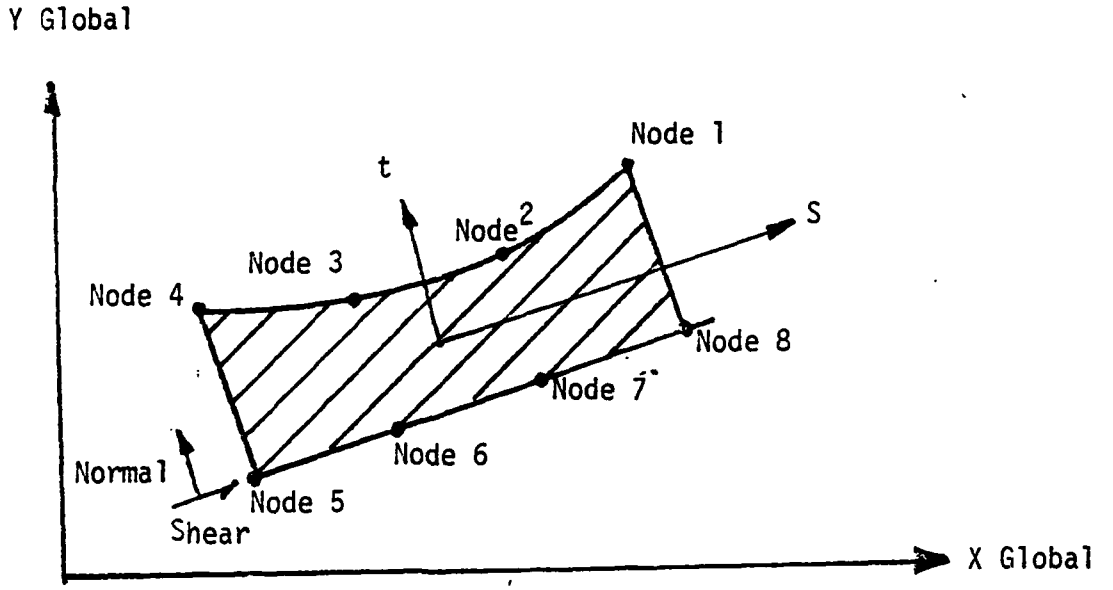

Figure 2.2.3-1 8-Node Distributed Spring

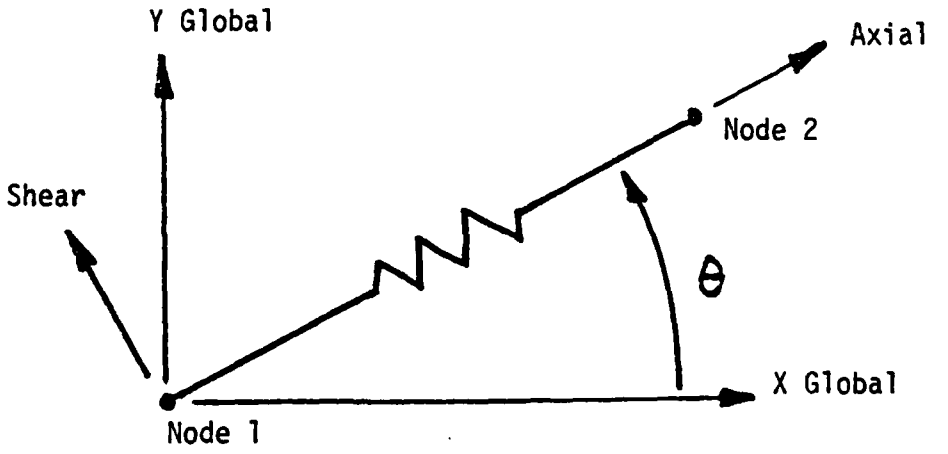

Figure 2.2.4-1 2-Node Concentrated Spring

defined normal to the first side. The subroutine converts these local values into global stiffnesses. The normal at the node point makes an angle with the global y-axis of:

$$\alpha = \text{Arctan}\left[\sum_j N_{j,s} Y_j / \sum_k N_{k,s} X_k\right] \qquad (2.2.3\text{-}1)$$

',s' refers to the partial derivative with respect to s.

The global stiffness components at a node become:

$$K_{Gx} = \cos^2 \alpha\, K_{Lx} + \sin^2 \alpha\, K_{Ly} \qquad (2.2.3\text{-}2)$$

$$K_{Gy} = \sin^2 \alpha\, K_{Lx} + \cos^2 \alpha\, K_{Ly} \qquad (2.2.3\text{-}3)$$

$$K_{Gxy} = \sin \alpha \cos \alpha\, (K_{Ly} - K_{Lx}) \qquad (2.2.3\text{-}4)$$

where:

K_{LX} = local axial stiffness at that node

K_{LY} = local shear stiffness at that node

Once the global stiffnesses are known, a reduced form of the integration described in Equation 2.2-7 can be performed. The thickness of the element in the t coordinate direction does not enter into the formulation. Therefore:

$$K = \int_{+1} K_G dS = \int_{-1} K_G(s) \frac{dS}{ds}\, ds = \sum K_{G_i}(s_i)_i \left|\frac{dS}{ds}\right|_i W \qquad (2.2.3\text{-}5)$$

where S is a measure of position along the spring element in the physical space and s is the corresponding position in the mapped space.

2.2.4 2-Node Concentrated Spring

The 2-node concentrated spring allows node-to-node connections, either axially or by shear. The stiffness matrix is determined explicitly from the global geometry.

In local coordinates the stiffness matrix is:

$$K = \begin{bmatrix} K_x & -K_x & 0 & 0 \\ -K_x & K_x & 0 & 0 \\ 0 & 0 & K_{xy} & -K_{xy} \\ 0 & 0 & -K_{xy} & K_{xy} \end{bmatrix} \qquad (2.2.4\text{-}1)$$

where

K_x is the axial stiffness
K_{xy} is the shear stiffness

and it operates in the nodal displacement vector where U and V refer to the local displacements at node 1 and node 2 (see Figure 2.2.4-1)

The stiffness matrix must be rotated into the global coordinate system. This is done explicitly to reduce the amount of formulation time required by the program:

$$K = \begin{bmatrix} K_{11} & -K_{11} & K_{12} & -K_{12} \\ & K_{11} & -K_{12} & K_{12} \\ & & K_{22} & -K_{22} \\ [SYM] & & & K_{22} \end{bmatrix} \qquad (2.2.4\text{-}2)$$

where:

$K_{11} = \cos^2 \theta K_x + \sin^2 \theta K_{xy}$

$K_{12} = \cos \theta \sin \theta (K_x - K_{xy})$

$K_{22} = \sin^2 \theta K_x + \cos^2 \theta K_{xy}$

θ = the angle between the local x axis and global x axis

2.2.5 Non-equilibration of Spring Elements

The development of the spring elements was intended to supply a

facility for modeling of both axial restraint and frictional shear. The axial restraint formulation is straightforward and widely documented. However, the generality of the formulation which includes shear stiffness results in an element which may cause non-equilibrating moments if the element has a finite thickness or length. Force equilibrium is, however, maintained unconditionally.

2.3 Nodal Coordinate Specification

There is limited, but very helpful, mesh generation capabilities in PAPST. In most models, only the corner nodes of the elements are required to define the geometry. Area elements, 12 and 9 nodes, can be specified with just 4 or 3 nodes. Intermediate side node numbers and coordinates are automatically generated at third point locations. (Note: This implies straight edges, curved edges must be explicitly specified.) The spring elements also have generation capabilities. Distributed springs can be specified with 2 or 4 corner nodes. If only 2 nodes are specified, the program will generate the other 2 corner nodes at the same global coordinates and ground them. Intermediate nodes are generated similar to the area elements. Concentrated springs can be specified with 1 or 2 nodes. If only one node is specified, the other node is generated at the same global coordinates and grounded. In the 2 node case, both nodes are not required to be attached to the area elements.

It is suggested that this facility be used whenever possible. If the user decides to specify the intermediate nodes, the third point spacing should be maintained. Actual coordinates may be input in either global rectangular or local polar coordinates. The program will convert all local specification to polar before the analysis begins.

2.4 Nodal Constraints

Nodes may have either of two types of displacement constraints, the displacement components at a node may be set explicitly, or they may be tied to those of another node. Both of these constraint types are set in the local coordinates (user specified) of the node or nodes.

2.4.1 Specified Displacements

The value of either or both dispacement components at a node may be explicitly set by the user. The following information refers to implementation of displacement specifications:

1) The structure must be constrained against rigid body rotation or displacement.

2) Axisymmetric problems are automatically constrained in the x-direction at the axis of symmetry. Only rigid body motion in the y-direction must be constrained by the user.

3) Constraints may be specified in local coordinates, enabling the user to model inclined supports.

4) Intermediate side nodes will be constrained automatically in accordance with the corner node constraints.

5) When solving symmetric crack problems, a symmetry constraint should be applied to the node corresponding to the crack tip as well as to other nodes on the plane of symmetry. Special constraints are required if the user if modeling tearing (see Section 2.6.4)

2.4.2 Tied Displacements

Up to 30 nodes in a set may be linked together to have common (but unknown) displacement components. Either degree of freedom at a node may be tied to that at another node. However, each degree of freedom may not be tied independently to separate nodes. Each node in the set must be in the same local coordinate system.

2.5 Loadings

Both mechanical and thermal loadings are available to the user. Concentrated forces at the nodes can be specified. Distributed tractions are converted to consistent nodal forces and corrected for large displacement effects. Temperatures at each of the nodes can be included in a thermal stress analysis. Pressures applied to a crack face include the singularity effect in the consistent nodal forces.

For elastic analysis only, all loads are imposed at full value. Thermal, load controlled, and displacement controlled analyses are all treated separately in plastic analyses. Thermal loadings, mechanical loads, and non-zero displacements cannot be handled concurrently in the plastic case. The program will handle in order of preference thermal, displacement, and mechanical loading, and ignore additional conflicting information if specified. Load factors defined in the non-linear analysis section (2.6.2) apply to the temperatures, the forces or the non-zero displacements.

2.5.1 Concentrated Nodal Loads

Concentrated forces can be applied in x and y components at each of the unconstrained nodal degrees-of-freedom. For axisymmetric problems, concentrated nodal loads are actually line loads which act on the complete circumference of the structure. Such loads are input on a load per radian basis. For example, if a load of 3 units per circumferential unit of length acts at a distance x from the axis of symmetry, the total force F is $3\ (2\pi x) = 6\pi x$. The required input load, on a per radian basis, is $F/2\pi$ or $3x$.

2.5.2 Distributed Tractions

Each element boundary can have distributed normal and/or shear tractions. The distribution of such tractions along the element edge can be completely general; however, most problems can be treated with a constant or linear variation. Normal tractions are positive when directed into the element, and shearing tractions are positive when acting in a counter-clockwise sense along the element edge. The program automatically computes the equivalent nodal loads for applied tractions. Consistent load generation is especially important in large deformation calculations since the load value and direction will change as the structure deforms.

Pressure loading can be specified along an element edge that is shared by two elements within the structure. The sign convention in this case will be determined by the direction implied in the nodal input. The program will "apply" the load on the element for which the nodal order matches the element specification.

2.5.3 Thermal Loading

For a thermal loading, temperature information must be provided at least at each of the corner nodes. If the temperatures are not given for some (or all) pairs of intermediate side nodes, PAPST will automatically set those values from a linear interpolation of the values at the corner nodes.

In certain thermal problems, an abrupt change in temperature may exist at an interface between elements, and thermal loading is desired for elements to one side of the interface but not for those on the other. In this case, it is necessary to use two different materials. The coefficient of thermal expansion should be set equal to zero for elements for which no thermal loading should be calculated.

PAPST has the capability to do thermal loading in both elastic and plastic analyses. In the elastic analysis, the thermal loading is combined with loads from pressures and imposed displacements. The plastic analysis, on the other hand, will not allow any other loadings to be applied and will override them if specified by the user. All of the non-linear input specifications remain unchanged, except now the load factors are applied to the temperatures.

Thermal loading affects two sections of the program, calculation of the strain components and body forces.

Thermally induced volumetric expansion must be subtracted from the strain increment in order to calculate the mechanical strain increment:

$$\Delta\epsilon^{mech} = \Delta\epsilon - \Delta\epsilon^{thermal} \qquad (2.5.3\text{-}1)$$

where the thermal strains are:

$$\Delta\epsilon^{thermal} = \alpha\Delta T \begin{bmatrix} 1 \\ 1 \\ 1 \\ 0 \end{bmatrix} \quad ; \qquad (2.5.3\text{-}2)$$

Thermal body forces are calculated when the element stiffness matrix is formed. These nodal forces are integrated over the element with the same Gaussian quadrature:

$$\Delta FB = \int_{\text{area}} B^T(U)C(U)\Delta\epsilon^{\text{f.b.}}(U)dA \qquad (2.5.3\text{-}3)$$

$$= \sum_i \sum_j (B^T C \ \Delta\epsilon^{\text{f.b.}} (\det J|)) \Big|_{S_i t_i} W_i W_j$$

where the shape functions and material properties are at the current values.

$$\Delta\epsilon^{\text{f.b.}} = \alpha\Delta T \begin{bmatrix} 1-D_{13}/D_{33} \\ 1-D_{23}/D_{33} \\ 0 \\ -D_{43}/D_{33} \end{bmatrix}$$

for plane strain

The D_{ij} terms in the plane strain case refer to the terms in the current material property matrix before they are modified for plane strain (see section 2.1.1).

2.6 OPTIONAL ANALYSES

The analyses contained in this section are special purpose developments to better model linear elastic and elastic-plastic fracture mechanics problems. Specifically covered are: stress intensity factor calculation (Reference 8), J-integral (Reference 1) calculation, and modeling of tearing (Reference 2).

2.6.1 Fracture Mechanics

The concept of enriching conventional elements with the asymptotic displacement field appropriate for fracture mechanics originated with Benzley. Extensive application has been made for both Mode I and Mode II in the elastic case. Implementation of the elastoplastic case is restricted to use in Mode I with the multilinear material model.

The approach is to add the leading terms in the asymptotic expansion to polynomial displacement field. This adds two extra unknowns to the set of nodal displacements of which one is zero for Mode I problems.

The asymptotic crack tip singular solution is described in the next section. The implementation of the combined mode enrichment is subsequently described with the Mode I formulation considered as a special case.

2.6.1.1 Asymptotic Crack Tip

The asymptotic displacement components at a crack tip are given in the standard polar coordinate system centered at the crack tip.

$$U = \frac{K}{2E}\sqrt{R/2\pi}\left[5 - 3\nu + \frac{7\alpha}{2} - 8\beta)\cos\frac{\theta}{2} - (1 + \nu + \frac{3\alpha}{2})\cos\frac{3\theta}{2}\right] \qquad (2.6.1.1\text{-}1)$$

$$V = \frac{K}{2E}\sqrt{R/2\pi}\left[(7 - \nu + \frac{13\alpha}{2} - 8\beta)\sin\theta/2 - (1 + \nu + \frac{3\alpha}{2})\sin\frac{3\theta}{2}\right]$$

For Mode II: (K_{II} only)

$$U = \frac{K}{2E}\sqrt{R/2\pi}\left[(9 + \nu - 8\beta)\sin\theta/2 + (1 + \nu)\sin 3\theta/2\right] \qquad (2.6.1.1\text{-}2)$$

$$V = \frac{K}{2E}\sqrt{R/2\pi}\left[-(3 - 5\nu - 8\beta)\cos\theta/2 - (1 + \nu)\cos 3\theta/2\right]$$

$$\alpha = \begin{cases} \text{slope of } \sigma\text{-}\varepsilon \text{ curve } \left(\dfrac{E\,\Delta\varepsilon - \Delta\sigma}{\Delta\sigma}\right) \\ \text{if plastic } K_p \\ 0 \text{ if elastic } K_I \end{cases} \qquad (2.6.1.1\text{-}3)$$

$$\beta = \begin{cases} 0 \text{ if plane stress} \\ (\nu + \alpha/2)^2/(1+\alpha) \text{ otherwise} \end{cases} \qquad (2.6.1.1\text{-}4)$$

$$\nu = \nu_{xy} \; ; \; E = E_x$$

with the angle measured from the crack line extension path.

2.6.1.2 Enriched Elements

The enriched quadrilateral element (Reference 9) has the same geometry as the standard elements. The displacement assumption used in the enriched element is essentially the usual displacement function plus the leading terms of the singular displacement expansion in Equation 2.6.1.1-1-2. It takes the form

$$u = \alpha_1 + \alpha_2 s + \alpha_3 t + \alpha_4 s^2 + \alpha_5 st + \alpha_6 t^2 + \alpha_7 s^3 + \alpha_8 s^2 t \qquad (2.6.1.2\text{-}1)$$
$$+ \alpha_9 st^2 + \alpha_{10} t^3 + \alpha_{11} st^3 + \alpha_{12} ts^3 + K_I f_1(s,t) + K_{II} g_1(s,t)$$

where α_i are undetermined coefficients

K_I, K_{II} are the stress intensities for Mode I and Mode II respectively

$f_1(s,t)$ $g_1(s,t)$ are based on the singularity equations (2.6.1.1-1,-2) and
evaluated in terms of the local mapped coordinates. A similiar expression exists for the v-component of displacement. In matrix form, Equation 2.6.1.2-1 may be written as

$$U(s,t) = P(s,t) + K_I f_1(s,t) + K_{II} g_1(s,t) \qquad (2.6.1.2\text{-}2)$$

By evaluating Equation 2.6.1.2-2 at each of the nodes, the following matrix equation may be written

$$U = C\alpha + K_I f_1 + K_{II} g_1 \qquad (2.6.1.2\text{-}3)$$

in which all matrices are known except U and α.

Solving for α then gives

$$\alpha = C^{-1}U - C^{-1}K_I f_1 - C^{-1}K_{II} g_1 \qquad (2.6.1.2\text{-}4)$$

Substituting for α then gives

$$U(s,t) = PC^{-1}U - PC^{-1}K_I f_1 - PC^{-1}K_{II} g_1 + K_I f_1(s,t) + K_{II} g_1(s,t) \qquad (2.6.1.2\text{-}5)$$

But as shown in Zienkiewicz, (Reference 37, page 106) the matrix of displacement interpolation functions i.e.,

$$\underset{1x12}{P} \quad \underset{12x12}{C^{-1}} = \underset{1x12}{N} = [N_1\ N_2\ N_3\ \ldots\ N_{12}] \qquad (2.6.1.2\text{-}6)$$

Consequently, Equation 2.6.1.2-5 may be written

$$u(s,t) = \Sigma N_i u_i + K_I[f_1(s,t) - \Sigma N_i f_{1_i}] + K_{II}[g_1(s,t) - \Sigma N_i g_{1_i}] \qquad (2.6.1.2\text{-}7)$$

where the second level subscripts indicate "evaluated at Node i." The analogous expression for the v-component of displacement is

$$v(s,t) = \Sigma N_i v_i + K_I[f_2(s,t) - \Sigma N_i f_{2_i}] + K_{II}[g_2(s,t) - \Sigma N_i g_{2_i}] \qquad (2.6.1.2\text{-}8)$$

Equations 2.6.1.2-7 and -8 are the displacement approximations used in the enriched element. It should be noted here, however, that in order to provide displacement continuity between the two element types, the second and third terms on the right-hand side should be multiplied by functions of

s and t which cause them to vanish on the boundary between enriched elements and conventional elements. Note also that the functions modifying the stress intensity factors multiplying $f_1(s,t)$, $f_2(s,t)$, $g_1(s,t)$ and $g_2(s,t)$ lead to functions of s and t in the 26 x 26 element stiffness matrix which cannot be numerically integrated with the same precision as the functions in the normal stiffness matrix. Specifically, 3 x 3 or 4 x 4 Gaussian quadrature integration is adequate for the conventional element whereas higher quadrature is required for accurate numerical integration of the enriched element and 8 x 8 integration is used. Higher order integration is not used for enriched elements in the nonlinear program. The significantly smaller enriched element used in the plastic analysis appears to obtain acceptable results using the standard 4 x 4 quadrature.

2.6.1.3 Additional Loading From Enrichment

The incorporation of the singularity displacement field has an effect on the loading at the crack tip. Both the distributed pressure and the thermal body forces must be modified to account for this added degree of freedom.

The pressure contribution takes the form:

(2.6.1.3-1)

$$\begin{aligned} P &= \int_0^r p\tilde{U}dr \\ &= r/2 \int_{-1}^{1} p\tilde{U}ds \\ &= r/2 \sum_j w_j \left(\sum N_i p_i\right)_j \tilde{U}_j \end{aligned}$$

when reduced to the Gaussian quadrature format, where:

(2.6.1.3-2)

$$\tilde{U}_j = \sqrt{r}\ \frac{4(1+\alpha-\beta)}{\sqrt{2\pi}} \left[\sqrt{\frac{1+S_j}{2}} - \sum_{i=2}^{4} N_i(S_j) \sqrt{\frac{i-1}{3}} \right]$$

where S_j is the local nodal coordinate of node j, and r is the length of the element edge to which the pressure is applied and the other variables are consistent with the notation in Section 2.6.1.1.

The thermal body force term at the crack tip is of the form:

$$\Delta FB^{*} = \int_{area} B^{*T}(U)C(U)\Delta\varepsilon^{f.b.}\,dA \qquad (2.6.1.3\text{-}3)$$

where the notation is consistent with Section 2.5.3 and 2.6.1.2.

2.6.1.4 Stress Intensity Factor Recovery

The solution of the set of governing equations for the global displacements also gives the normalized stress intensity factors. Recovery of the actual stress intensity factors becomes trivial:

$$K_I = E_x\, U_I \qquad (2.6.1.4\text{-}1)$$

$$K_{II} = E_x\, U_{II} \qquad (2.6.1.4\text{-}2)$$

Having the stress intensity factors enable us to calculate the strain energy release rate at the crack tip (G in elasticity is comparable to J in plasticity). The following equations are for cracks in orthotropic materials that are aligned with the principal material axes. Since the program will only accept material properties in global coordinates, this restricts the orientations to $\emptyset^{\circ}$ and 90°. The equations reduce to isotropic unconditionally (Reference 38).

$$G_I = K_I^2 \left[\frac{D_{11}D_{22}}{2}\right]^{1/2} \left[\left(\frac{D_{22}}{D_{11}}\right)^{1/2} + \frac{(2D_{12} + D_{44})}{2D_{11}}\right]^{1/2} \qquad (2.6.1.4\text{-}3)$$

$$G_{II} = K_{II}^2 \left[\frac{D_{11}}{\sqrt{2}}\right] \left[\left(\frac{D_{22}}{D_{11}}\right)^{1/2} + \frac{(2D_{12} + D_{44})}{2D_{11}}\right]^{1/2} \qquad (2.6.1.4\text{-}4)$$

2.6.2 J-Integral

The J-integral (Reference 2) is a measure of the amplitude of the near crack tip stress and strain fields in an elastic-plastic material. It has been proposed as a fracture initiation criterion. Under conditions of small scale yielding for which linear elastic fracture mechanics is applicable, J reduces to the energy release rate G. It is related to the Mode I stress intensity factor by

$$J = \begin{cases} K_I^2/E & \text{for plane stress} \\ (1-\nu^2)\ K_I^2/E & \text{for plane strain} \end{cases} \qquad (2.6.2\text{-}1)$$

The J-integral for elastic-plastic crack problems is given in terms of the strain energy density:

$$W = \int_0^{\varepsilon_{ij}} \sigma_{ij} d\varepsilon_{ij} \qquad (2.6.2\text{-}2)$$

as

$$J = \int_\Gamma (W dy - T_i \frac{\partial U_i}{\partial x} ds) \qquad (2.6.2\text{-}3)$$

where the crack lies along the local x axis and the contour is traversed counterclockwise from one crack face to the other. Figure 2.6.2-1 shows the general contour. The traction vector has components T_i and the corresponding displacement components are U_i. The differential length along the arc is indicated by ds.

In the case of finite elements, a path must be traversed along the element boundaries. Typical path contours are shown in Figure 2.6.2-1. The integral is performed using the averaged nodal stresses and strains and a line Gaussian quadrature integration. The use of averaged values avoids any element or path dependence.

The J-integral is calculated as follows:

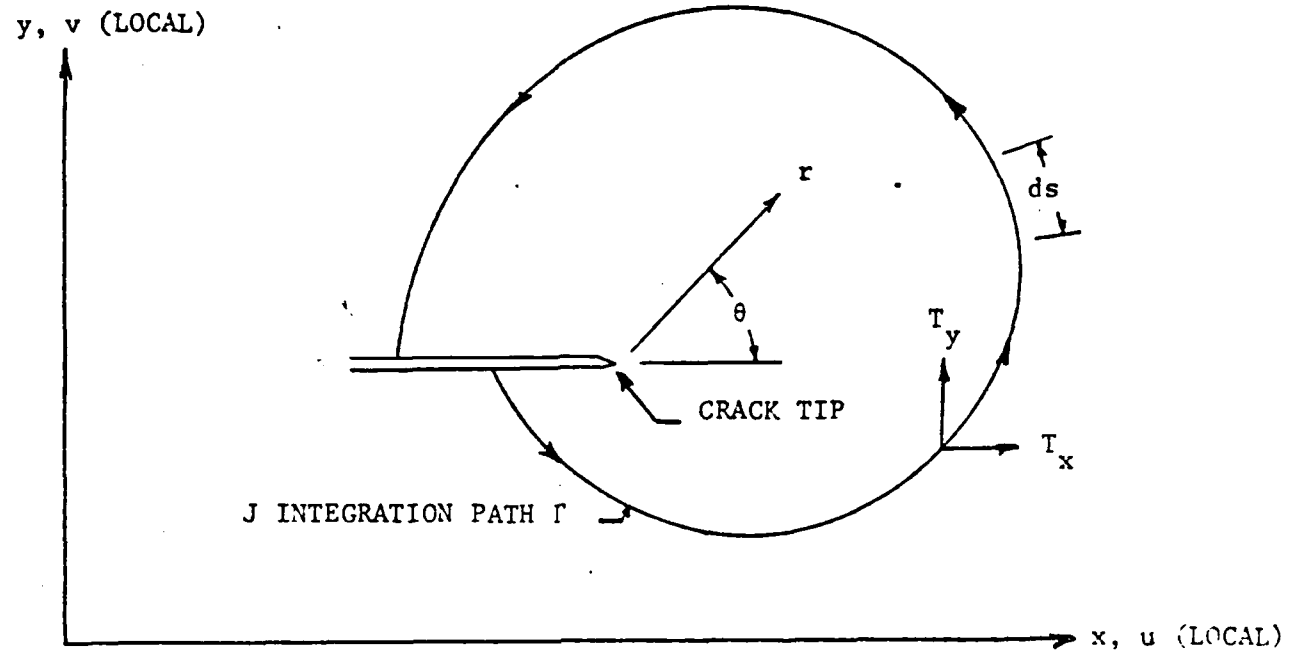

Polar Coordinate System at Crack Tip and a Contour for the J Path Integral

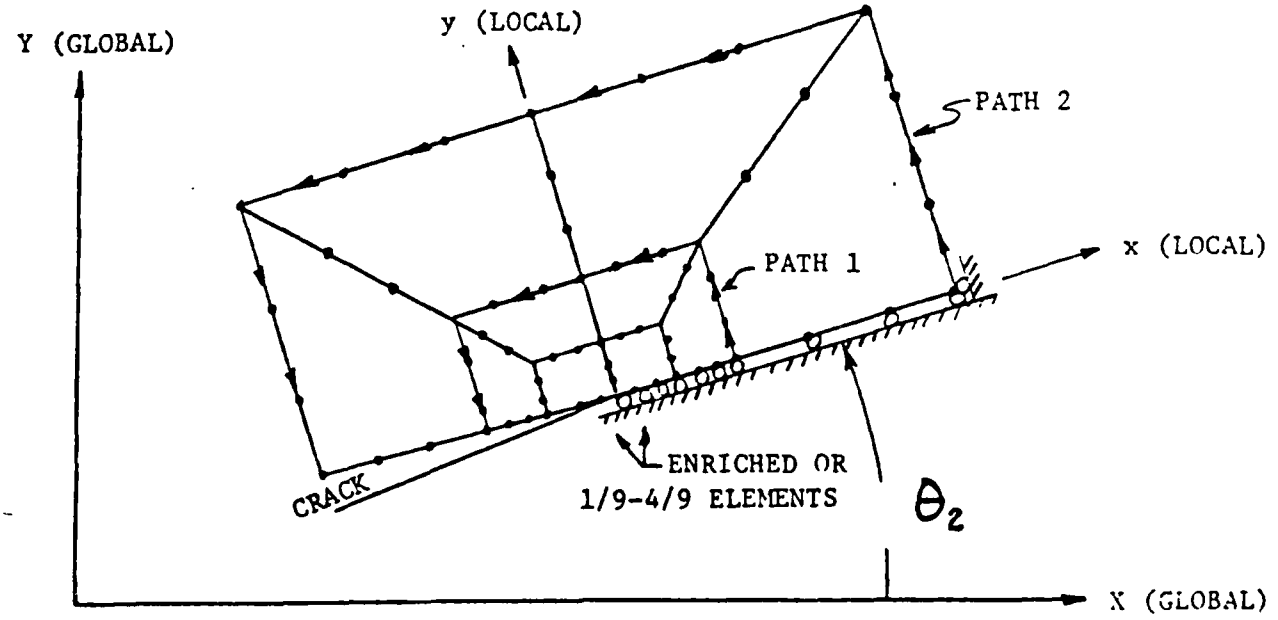

Two Typical Contours Γ for Evaluation of J in a Finite Element Mesh

Figure 2.6.2-1 Contours for Evaluation of the J-Path Integral

$$J = \sum_{\text{edges}} \int_s [\sin \theta_2(\sigma_{xy} \quad U,_y + \sigma_y \varepsilon_y - W) + \cos \theta_2(\sigma_{xy} \cdot \varepsilon_x + \sigma_y \quad V,_x)] \, dx + [\cos \theta_2(W - \sigma_x \varepsilon_x - \sigma_{xy} V,_x) - \sin \theta_2(\sigma_x U,_y + \sigma_{xy} \varepsilon_y)] \, dy \tag{2.6.2-4}$$

where: (for power hardening materials)

$$W = \frac{1}{E}\left[\frac{(1+\nu)}{3}\sigma_e^2 + \frac{(1-2\nu)}{6}\sigma_{pp}^2 + \frac{n}{n+1}\alpha\left(\left(\frac{\sigma_e}{\sigma_{yd}}\right)^{n+1} - 1\right)\sigma_{yd}^2\right] \tag{2.6.2-5}$$

(for multilinear materials)

$$W = \frac{1}{E}\left[\frac{(1+\nu)}{3}\sigma_e^2 + \frac{(1-2\nu)}{6}\sigma_{pp}^2 + \sum^{m-1} \frac{\alpha_i}{2}(\sigma_{i+1}^2 - \sigma_i^2) + \frac{\alpha_n}{2}(\sigma_e^2 - \sigma_m^2)\right] \tag{2.6.2-6}$$

and:

$$\sigma_{pp} = \sigma_{xx} + \sigma_{yy} + \sigma_{zz} \tag{2.6.2-7}$$

$$\nu = \nu_{xy}$$

$$E = E_x$$

An additional contribution must be included for the axisymmetric J-integral (Reference 10):

$$J_{area} = \int_A [\cos \theta_2(\sigma_z \varepsilon_z - \sigma_x \varepsilon_x - \sigma_{xy} V,_x)/z + \sin \theta_2(\sigma_x U,_y - \sigma_{xy} \varepsilon_y)/z] \, dA \tag{2.6.2-8}$$

This area integral is added to the contour integral for all elements that fall within the path contour, i.e.,

$$J = J_{path} + J_{area} \tag{2.6.2-9}$$

The energy release rate defined in Section 2.6.1.4 can use the plastic singularity to approximate the J value for a multilinear material model. If K_p is substituted for K_I in equation 2.6.1.4-3, G_I becomes J_p with the following modifications:

For plane stress:

$$J_p = (1 + \alpha)\, G_I \qquad (2.6.2\text{-}10)$$

For plane strain:

$$J_p = \frac{[1 + \gamma^2/2 - 3\nu\gamma/2 + \alpha_m(1 - 3\gamma/4 + \gamma^2/2)]}{(1 - \nu^2)}\, G_I \qquad (2.6.2\text{-}11)$$

where:

$$\gamma = (\nu + \alpha_m/2)/(1 + \alpha_m) \qquad (2.6.2\text{-}12)$$

and α_m is the slope of the last ligament of the plastic stress-strain relationship defined by equation 2.1.4-1

2.6.3 Tearing Modulus

The applied Tearing Modulus[14] is defined by

$$T_{APPL} = \frac{E}{\sigma_o^2}\,\frac{dJ}{da} \approx \frac{E}{\sigma_o^2}\,\frac{\Delta J}{\Delta a} \qquad (2.6.3\text{-}1)$$

E is Young's modulus, σ_o is the flow stress (average of yield and ultimate stresses), and dJ/da represents the rate of change of the J-integral with respect to crack length. Ductile crack growth stability is assessed using the tearing modulus as follows: Fracture is stable upon reaching J_{IC} if $T_{APPL} < T_{MATL}$, or unstable if $T_{APPL} > T_{MATL}$, where T_{MATL} is the tearing modulus of the material taken from test records (resistance curves) of J versus Δa in standard J_{IC} tests.

Finite element analysis including crack growth (Reference 11) can be performed to calculate T. In PAPST, crack extension over one element can be analyzed. This is done by inserting a very stiff distributed spring along the path defined for crack growth. The user is allowed to define the J_{IC} value at which the crack should grow. Once this value is reached, the spring is progressively softened holding all other boundary conditions fixed. When the program converges, a new value for J is computed. The Tearing Modulus can then be calculated from Equation 2.6.3-1.

2.7 OPTIONAL FEATURES

Several optional features are available in the program to aid the user in describing the model and interpreting the results. This section describes the user selectable features.

2.7.1 Plotting

The plotting package has the following capabilities:

a) Drawing deformed shape

b) Stress contour plots

c) Thermal contour plots

d) Enlargement of Selected Regions

This package has been developed for use on a CALCOMP plotter.

2.7.2 Wavefront Reordering

This feature is still in development. The user can, however, utilize the manual reordering feature. This allows the frontal solution to be performed in a different order from the element input ordering. See Appendix A, Topic 6, Subject C for details.

2.8 REFERENCES

1. Rice, J.R. and Rosengren, G.F., "Plane Strain Deformation Near a Crack Tip in a Hardening Material," J. Mech. and Physics of Solids, Vol. 16 No. 1, pp 1-12, 1968.

2. Paris, P.C., Tada, H., Zahoor, A., and Ernst, H., "The Theory of Instability of the Tearing Mode of Elastic-Plastic Crack Growth," in Elastic-Plastic Fracture, ASTM Special Technical Publication 668, pp 5-36, pp 251-265, 1979.

3. Gifford, L.N., "APES-Second Generation Two-Dimensional Fracture Mechanics and Stress Analysis by Finite Elements," DTNSRDC Report 4799, Dec. 1975.

4. Gifford, L.N., "APES-Finite Element Fracture Mechanics Analysis: Revised Documentation," DTSRDC Report 79/023, Mar 1979.

5. Hilton, P.D., Gifford, L.N., "Elastic-Plastic Finite Element Analysis for Two Dimensional Crack Problems," ASTM Symposium on Elastic-Plastic Fracture Mechanics, October, 1981.

6. Praeger, W., Introduction to Mechanics of Continua, Dover Press, 1971, pp. 154-156.

7. Zienkiewicz, O.C., The Finite Element Method in Engineering Science, McGraw-Hill, London (1971).

8. Sih, G.C. and H. Liebowitz, Chapter 2, "Mathematical Theories of Brittle Fracture," Fracture An Advanced Treatise, Academic Press, New York (1968).

9. Gifford, L.N. and Hilton, P.D., "Stress Intensity Factors by Enriched Finite Elements," Eng. Fracture Mech., Vol. 10, No. 3, pp 485-496, 1978.

10. Bergkvist, H. and Lan Huong, G., "J-Integral Related Quantities in Axisymmetric Cases," Int. J. of Fracture, Vol. 13, No. 4, pp 556-558, August 1977.

11. Shih, C.F., deLorenzi, H.G., and German, M.D., "Crack Extension Modeling with Singular Quadratic Isoparametric Elements," Int. J. Fracture 12, pp 544-548, 1977.

12. Nayak, G.C. and O.C. Zienkiewicz, "Elastic-Plastic Stress Analysis - A Generalization for Various Constitutive Relations Including Strain Softening," Int. J. for Numerical Methods in Engineering, Vol. 5, No. 1, 1972, pp. 113-135.

13. Hill, R., The Mathematical Theory of Plasticity, Oxford University Press, London (1956).

14. Gifford, L.N., "J-Integral Analysis of a Compact J_{IC} Specimen," DTNSRDC Structures Dept. Technical Report m-4, September, 1978.

15. Joyce, J.A. and M.G. Vassilaros, "An Experimental Evaluation of Tearing Instability Using the Compact Specimen," Proceedings of the Thirteenth National Symposium on Fracture Mechanics, ASTM-STP 743, P. 525-542 (1981).

16. Wang, C., Applied Elasticity, McGraw-Hill, New York (1953).

17. Nayak, G.C. and Zienkiewicz, O.C. "Note on the 'Alpha' - Constant Stiffness Method for Analysis of Nonlinear Problems," Int. J. for Numerical Methods in Engineering Vol. 4, 1972, pp. 579-582.

18. Gifford, L.N. and Hilton, P.D., "Preliminary Documentation of PAPST-Nonlinear Fracture and Stress Analysis by Finite Elements," DTSRDC, Structures Dept. Technical Report M-43 (January 1981).

3.0 VERIFICATION

Verification of a computer program is an on-going process. Each new feature or modification to the program must be shown to work itself and be shown to not affect the performance of other existing features of the program. Considering the amount of modification that has been made to PAPST during this contract, it was appropriate to collect and review the previous verificatioon cases. From this collection, selected test cases were used to baseline this version against previous versions to see what differences, if any, existed, and if they did, were they a result of improvements and modifications. New features, such as springs and tearing, required verification to theoretical or experimental results.

This verification effort was not exhaustive. There are many features and combinations of features that have not been explicitly verified. Experience with the program, both here and at the Navy, leads us to believe that there are no obvious problems or errors.

3.1 General Topics

3.1.1 Elastic Analysis

This version of PAPST was developed from the most recent version of APES. The broad base of experience with the use of APES, which is now fully incorporated, implies that this section of the program is partially verified. Also, efforts required in later portions of this section require that the elastic solution be correct. Therefore, no specific effort was undertaken to verify this topic.

3.1.2 Elastic Singularities

In Section 3.5 one of the comparisons to verify the J-integral involved the use of the elastic singular solution. The results from the elastic singular solution were found to be consistent with previously reported values.

3.1.3 Multiple Runs

Several of the verification test cases were run sequentially through the program. Included were multiple elastic and multiple elastic/plastic cases as well as combinations of elastic and elastic/plastic cases. All of the problems ran identical to cases run individually.

3.1.4 Inclined Supports

Rotated test cases, similar to the J_{IC} test cases used in Section 3.5, were generated and run to verify that the solution was insensitive to the model orientation. Table 3.1-1 summarizes the results. Overall comparison is excellent. The only noticeable discrepancy arises from the plastic singularity, and this was expected because it is not generally accurate.

TABLE 3.1-1

COMPARISON OF INCLINED MODEL TO UNROTATED MODEL

DESCRIPTION		$\theta=0^{\circ}$	$\theta=45^{\circ}$	$\Delta\%$
Model #1 - 6EL, Plastic, Plane Strain				
Incr. #1	PFRAC (1)	1.312940	1.312767	-*
	Highest Loaded Node	62038.339	62040.306	-
	J_1	85.010	85.003	-
	J_2	65.263	65.256	.011
Incr. #2	Highest Loaded Node	110050.114	111451.825	1.27
	J_1	803.70	776.55	3.378
	J_2	696.78	690.79	0.86
Incr. #3	Highest Loaded Node	139335.383	140941.39	1.15
		2079.0	2048.7	1.46
		1690.06	1682.8	0.43
Model #2 - 6EL, Plastic, Plain Strain, Enriched				
Incr. #1	PFRAC (1)	1.244933	1.244870	-
	K_p	5103.45	5703.87	-
	J_1^p	77.103	77.108	-
	J_2	62.876	62.878	-
	Highest Loaded Node	85189.317	85210.081	.02
Incr. #2	K_p	28066.948	30595.377	9.01
	Highest Loaded Node	130250.355	133047.625	2.15
	J_1	803.75	775.62	3.5
	J_2	689.61	683.47	0.89
Incr. #3	K_p	57500.24	60063.13	4.46
	Highest Loaded Node	174047.27	176820.054	1.59
	J_1	2066.7	2033.5	1.61
	J_2	1743.8	174.06	0.81

* <.01%

3.2 Concentrated Springs

The concentrated spring verification addresses each of the possible uses of the spring. Features of the spring are:

1) Axial and shear stiffness
2) 1-node - grounded (zero length)
3) 2-node - between element
4) Rotated or inclined specification
5) Combined stiffness action
6) Potential violation of moment equilibrium

Four test cases were developed to cover all of these topics. Three of the cases are statically determinate, permitting easy checking. The fourth case demonstrates the problem with moment equilibrium.

Test Case #1, shown in Figure 3.2-1, is one element that is pinned at one end and restrained by a spring at the other. An overturning force is applied. The spring was defined by one node, resulting in the grounding of the other end and zero length. Only the shear stiffness was input. The local coordinate system defaults to the global system and thereby defines a spring with vertical stiffness only.

Test Case #2, shown in Figure 3.2-1, places an axial spring between two elements. Both elements are restrained from vertical motion. The left element is pinned at the far side and the right element has a uniform traction applied. The force from the traction must be transferred through the spring to the far support. Stabilizing moments at the base of each element were checked for equilibrium.

Test Case #3, shown in Figure 3.2-2, has an axial spring that is defined between two pinned supports. One of the supports undergoes a known displacement. Resultant spring forces are axial.

Test Case #4, shown in Figure 3.2-2, has the same model geometry as Test Case #3. The difference is that both the axial and shear stiffnesses were set to the same value. This results in an equal restraint against motion in all directions. The force at the displaced end of the spring is the spring stiffness times the displacement. No other forces are developed. The other end of the spring has a support reaction that is equal and opposite to the force developed at the displacement. Therefore, moment equilibrium is not maintained over the finite length of the spring.

The computer runs that were made agree completely with the analyses shown in Figures 3.2-1 and 3.2-2.

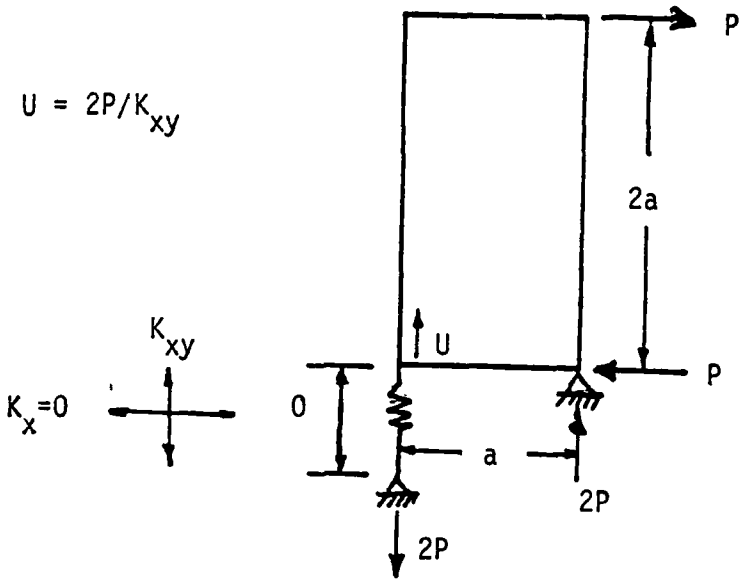

Example #1 Grounded and Shear

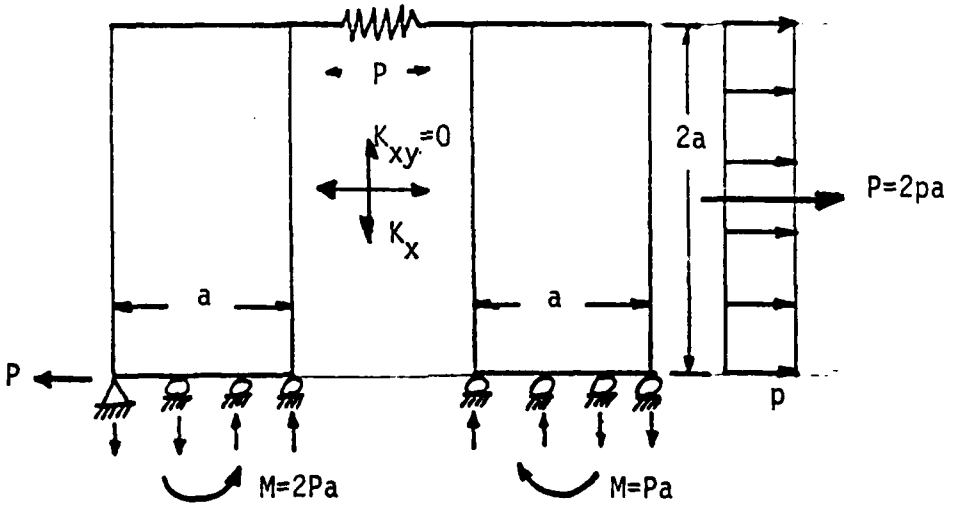

Example #2 Between Elements and Axial

Figure 3.2-1 Concentrated Springs - Examples #1 and #2

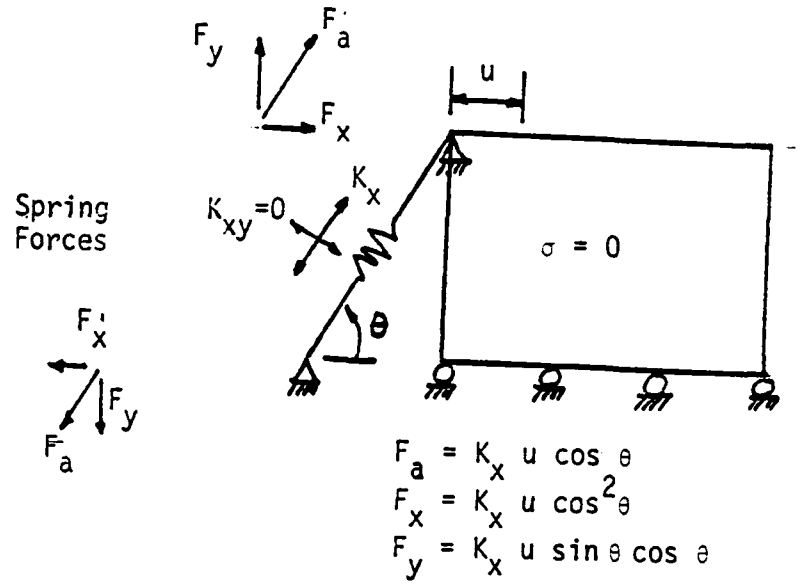

$$F_a = K_x\, u \cos\theta$$
$$F_x = K_x\, u \cos^2\theta$$
$$F_y = K_x\, u \sin\theta \cos\theta$$

Example #3 Axial and Rotated

$$K_x = K_{xy} = K$$

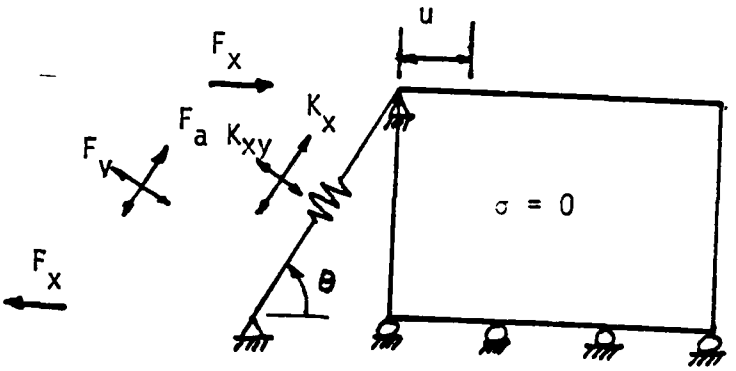

$$F_x = K\, u$$
$$F_z = K\, u \cos\theta$$
$$F_v = K\, u \sin\theta$$

Example #4 Combined and Rotated

Figure 3.2-2 Concentrated Springs - Examples #3 and #4

3.3 Distributed Springs

The distributed spring verification is similar to that for the concentrated spring. Most of the possible uses and features were tested. However, the added complexity of the distributed spring makes an identical level of study impractical. Only the most common features are addressed, and we rely on the generality of the derivation to cover other, less common cases.

Features of the springs are:

1) Axial and shear stiffness
2) 2-node - grounded (intermediate nodes generated)
3) 4-node - between element (intermediate nodes generated)
4) Rotated or inclined specification
5) Combined stiffness action
6) Potential violation of moment equilibrium

Three test cases were developed to cover these topics. The one case that demonstrates the potential violation of moment equilibrium is statically determinate if this is kept in mind. The other two can be quickly analyzed by hand.

Test Case #1, shown in Figure 3.3-1, is a row of elements resting on an elastic foundation provided by the springs. Uniform suction is applied to the top surface. The springs are defined by 2 nodes and, therefore, have zero length and are grounded. Axial stiffness in this case corresponds to a vertical restraint. The distribution of pressure on the top surface is reproduced in the reactions provided by the springs.

Test Case #2, shown in Figure 3.3-2, is the same general configuration as Test Case #1. Rather than suction, uniform shear is applied to the top surface. Vertical restraints are defined along the bottom edge of the elements. The springs have a finite length and only a shear stiffness. Deformation of the elements causes some small redistribution of shear force to the springs. The moment developed by the vertical restraint counterbalances the moment caused by the shear force. However, this moment has a magnitude that implies that the springs are supplying the reaction at the point of connection to the element and not at the ground of the springs. This is consistent with the warning on the violation of moment equilibrium. The formulation of the spring does not account for length, and therefore, shear springs of finite length will not balance properly.

Test Case #3, shown in Figure 3.3-3, demonstrates the use of the spring between elements. Two elements are connected by a spring on an inclined surface. Suction is applied to the unsupported element and must be transferred through the spring to the other element to reach a support. The moment developed at the support balances the moment from the suction. Equal axial and shear stiffnesses provide a uniform stable connection between the two elements. A biased connection could be specified by the use of different spring stiffnesses for axial and shear components.

Computer runs made for these cases agree completely with the analyses shown in Figures 3.3-1 through 3.3-3.

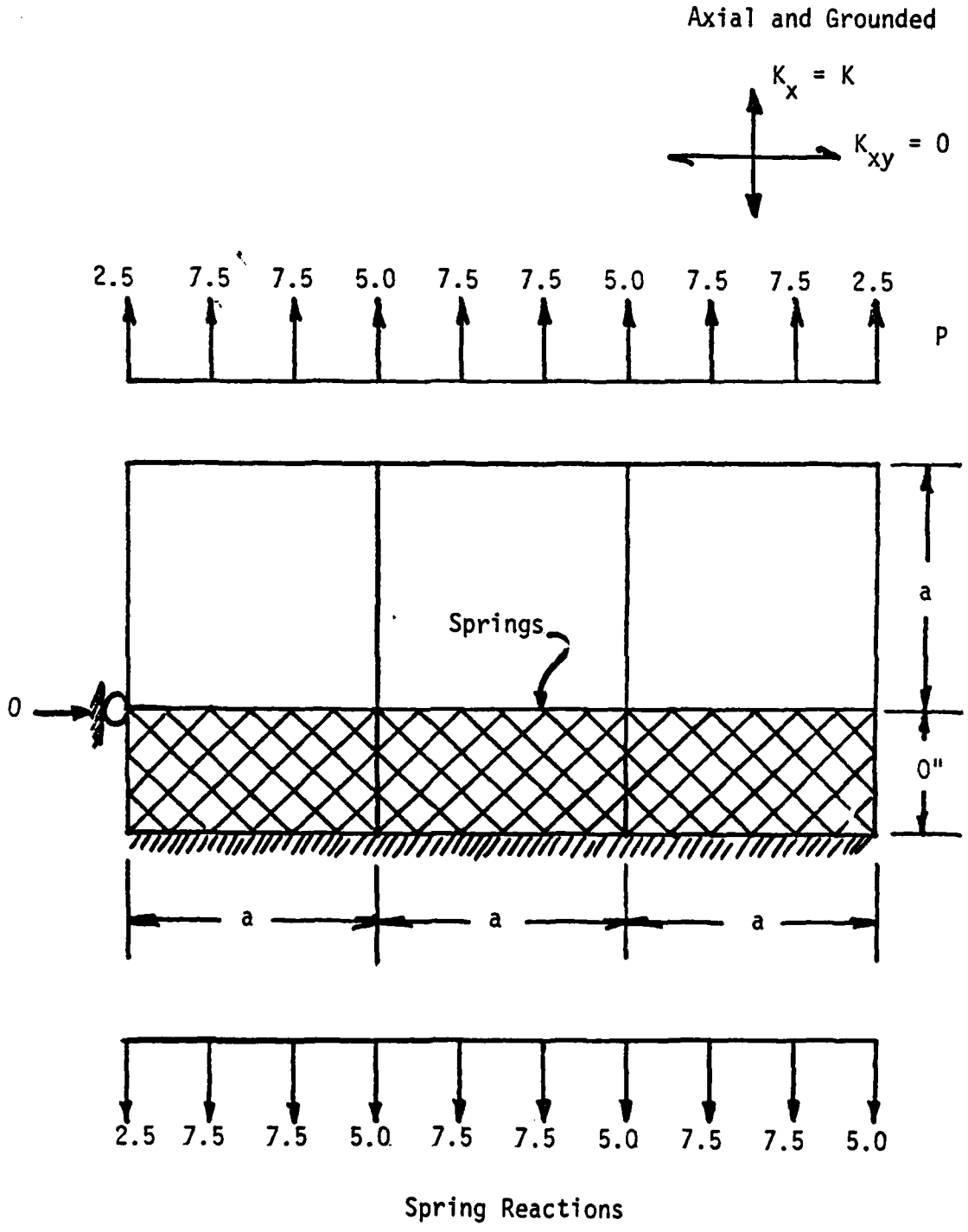

Figure 3.3-1 Distributed Springs - Example # 1

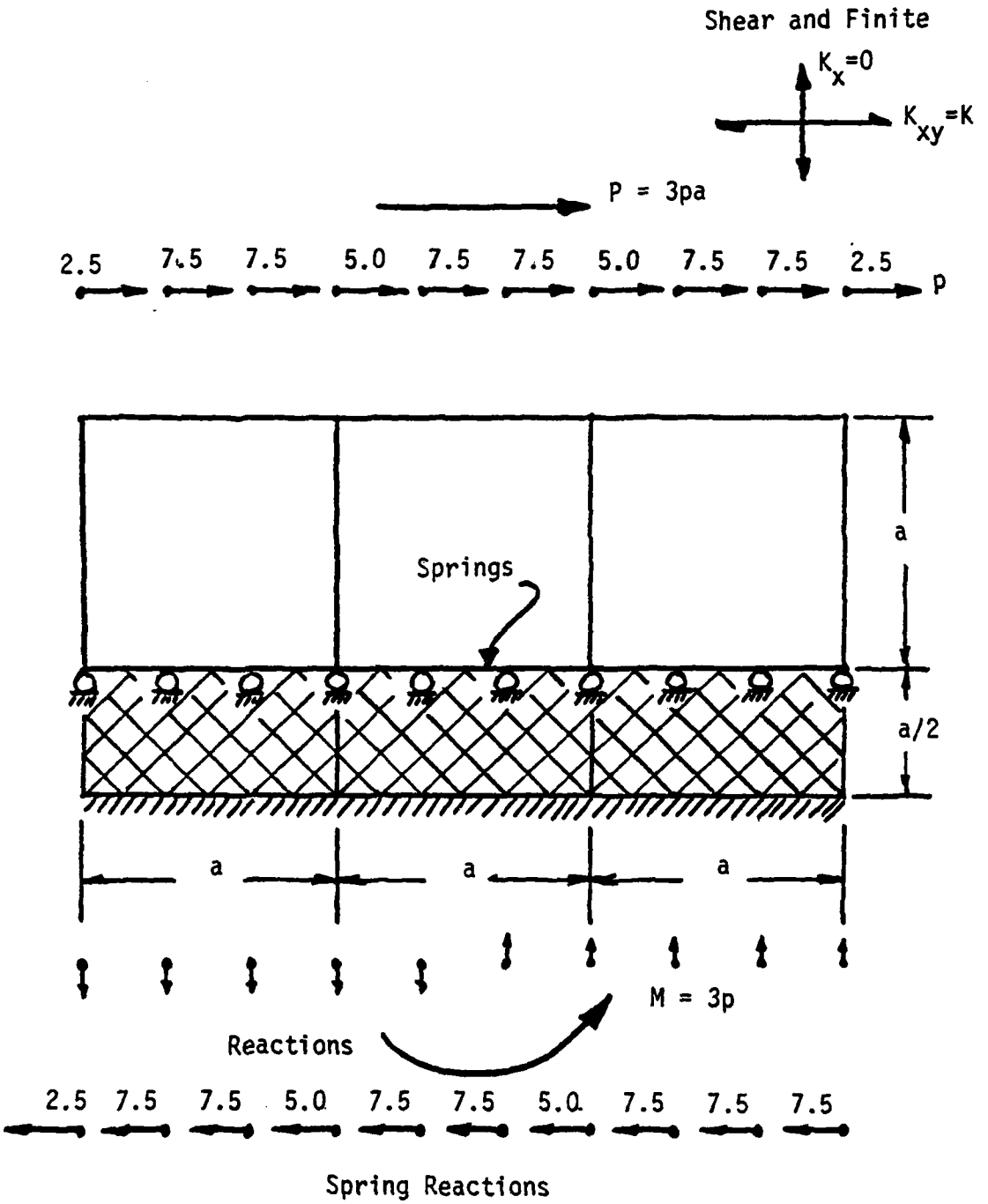

Figure 3.3-2 Distributed Springs - Example #2

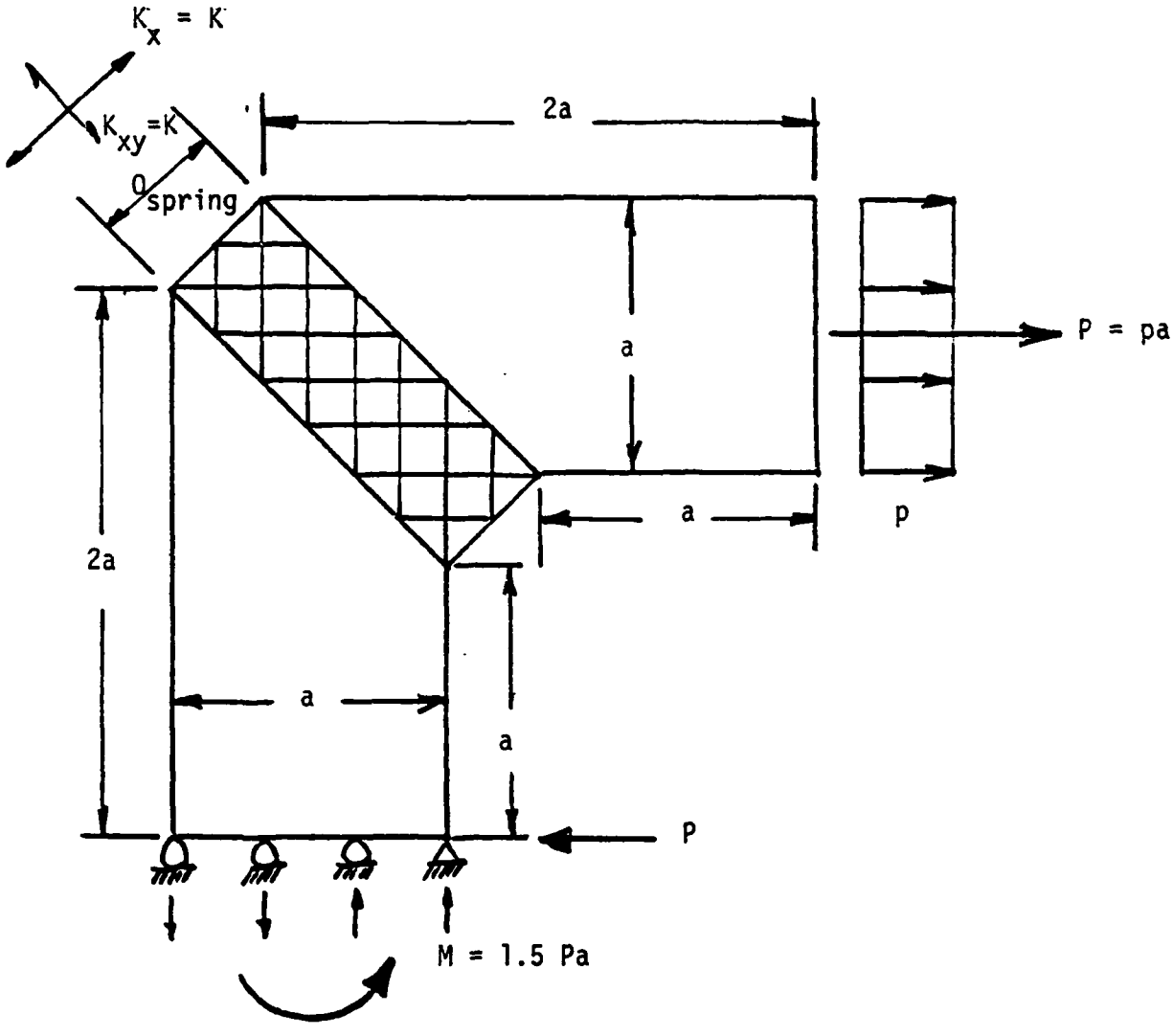

Figure 3.3-3 Distributed Springs - Example #3

3.4 Thick Walled Cylinder

The plane strain idealization of an internally pressurized thick walled cylinder (an axisymmetric problem) is shown in Figure 3.4-1. This problem was employed to verify the previous version of PAPST. The method of load incrementation, convergence characteristics, displacements at the inside and outside surfaces are all indicated in Table 3.4-1 and comparison is made with the results of Reference 12. We have added the results from the present PAPST program to Table 3.4-1.

In order to also correlate these results to analytic example, we limited the analysis to the small scale displacement option. The outer displacement of an elastic/perfectly plastic cylinder can be approximated for a Von Mises yield criteria from work done by Hill (Reference 13). The elastic/plastic boundary can be found by the equation.

$$P/\sigma_{yd} = \ln(c/a) + 1/2(1 - c^2/b^2) \qquad (3.4\text{-}1)$$

where:

a = internal radius
b = external radius
c = elastic/plastic interface radius a $\leq$ c $\leq$ b
p = internal pressure
σ_{yd} = yield stress x 2/ $\sqrt{3}$ to account for Von Mises criterion rather than Tresca.

The displacement field in the elastic region then becomes:

$$U = \frac{(1+\nu)}{2E}\,\sigma_{yd}\,\frac{c^2}{b^2}\left((1-2\nu)r + b^2/r\right) \qquad (3.4\text{-}2)$$

where:

E = Young's modulus
ν = Poisson's ratio
r = radius to be evaluated

Results for this equation are compared to the computed results on Table 3.4-1.

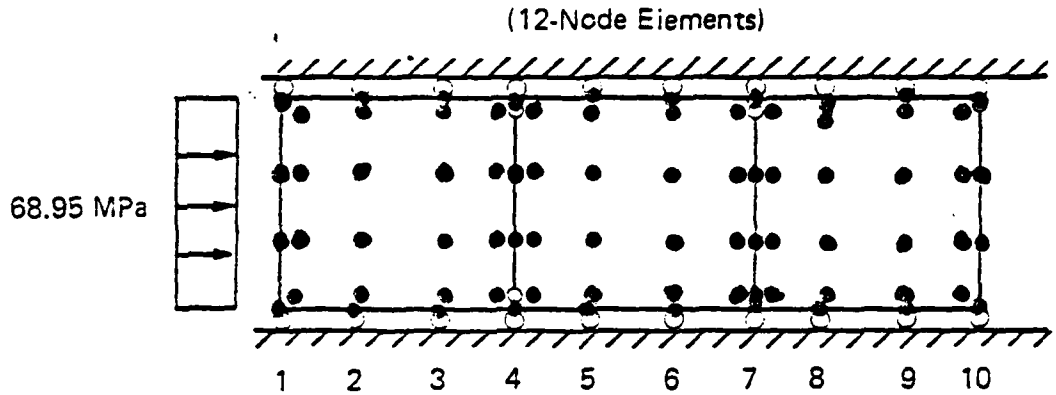

ϵ (Young's Modulus) = 6.895 $(10)^4$ MPa

ν (Poisson's Ratio) = 0.33

σ_{yd} (Yield Stress) = 68.95 MPa Elastic – Perfectly Plastic $\sigma - \epsilon$ Curve

Approximate Locations of Integration Points at which Stress-Strain History is Monitored are Shown by Dots

Figure 3.4-1 Idealization of Thick Wall Cylinder for Plastic Analysis

TABLE 3.4-1

RESULTS FOR 3 ELEMENT IDEALIZATION OF THICK WALLED CYLINDER

Increment Number	Internal Stress / Yield Stress	Small Scale Displ. Theory (Ref. 13)	Small Scale Displ. Initial Stress (Ref.17)	Large Scale Disp. New Papst	Large Scale Disp. New Papst	Large Scale Disp. Old PAPST (Ref. 18)
1	0.453		NA	1	1	2 (1)
				.261	.261	.262 (2)
		.1616		.161	.161	.162 (3)
2	0.5		3	2	2	2
			.294	.294	.294	.294
		.1811	.181	.181	.181	.181
3	0.55		3	2	2	2
			.332	.337	.337	.338
		.2053	.203	.206	.206	.206
4	0.6		4	2	2	2
			.391	.387	.387	.388
		.2348	.236	.234	.235	.235
5	0.65		4	2	2	2
			.455	.456	.456	.457
		.2723	.272	.272	.272	.273
6	0.7		5	3	3	3
			.546	.546	.547	.549
		.3215	.321	.321	.321	.323
7	0.75		6	3	3	3
			.688	.689	.691	.696
		.3951	.395	.396	.397	.400
8	0.77		7	3	3	3
			.770	.775	.781	.787
		.4391	.438	.440	.444	.447
9	0.79		8	3	3	3
			.898	.923	.936	.950
		.5094	.504	.516	.523	.531

(1) Number of iterations to convergence
(2) Radial displacement at inside surface, in x 10^2
(3) Radial displacement at outside surface, in x 10^2

3.5 J-Integral - Compact J_{IC} Specimen

A limited amount of verification of the option has been performed to assess the validity of the J integral calculation. The previous revision of PAPST had extensive testing and was subjected to correlation with alternate solutions (Reference 14). While the calculation procedure has been completely rewritten, the basic equations and approach remain unchanged.

A single model was chosen to compare against previous results. The geometry of the model is shown in Figure 3.5-1. It is approximately the same as the geometry used for Reference 14.

Three separate cases were analyzed: elastic enriched, plastic, and plastic enriched. The cases were run for both plane strain and plane stress. Results for these runs are summarized in Table 3.5-1. Comparable results are also shown for calculations done with the previous revision of Papst (Reference 14).

P = 40 ksi
and
p = 60 ksi

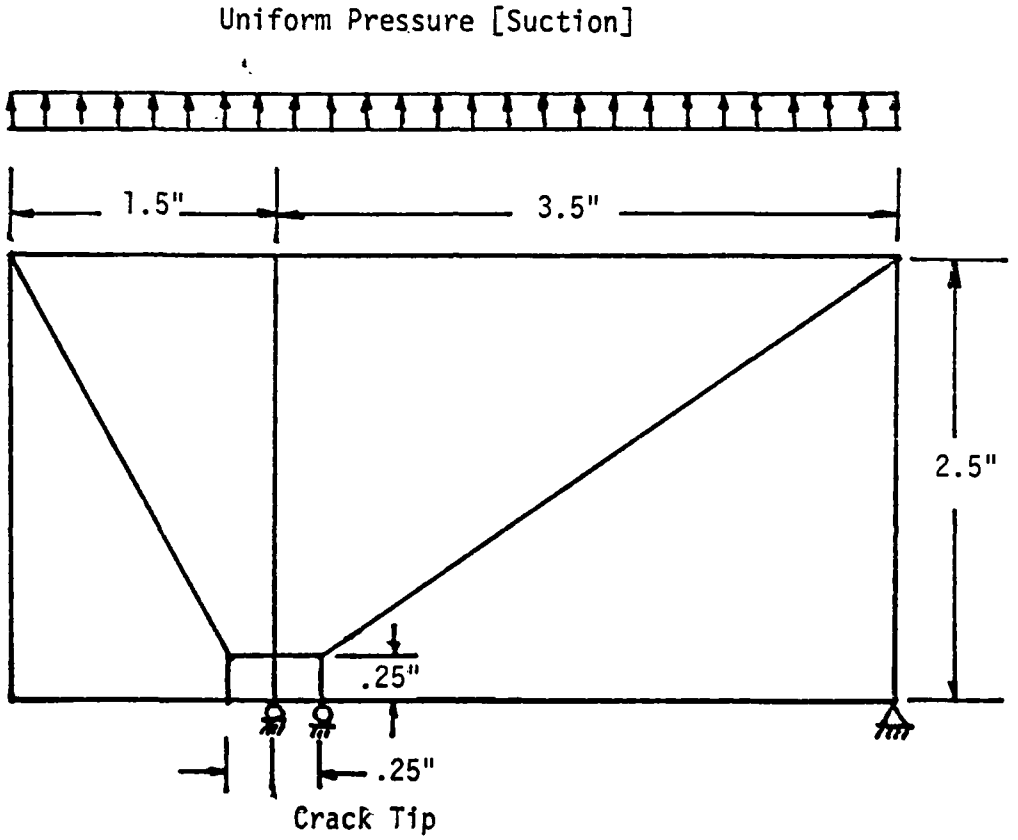

$E = 30 \times 10^6$ psi

$\nu = .3$

$\sigma_{yd} = 100{,}000$ psi

$\alpha = 10$

$n = 1$

$\beta = 0.0$

Plane Stress
and
Plane Strain

Figure 3.5-1

TABLE 3.5-1

COMPARISON OF J-INTEGRAL RESULTS FROM NEW AND OLD PROGRAMS

		Description	P=40KSI			P=60 KSI		
			J_{ssy}	J_s	J_p	J_{ssy}	J_s	J_p
Old PAPST (ref)	Plane Stress	6 EL, Powder Hardening w/core	851	430	1030	1920	1500	2750
		6 EL, Bilinear	-	-	822	-	-	2140
		14 EL, Bilinear	-	-	801	-	-	1990
		6 EL, Bilinear Enriched	814	211	835	1830	857	2180
		14 EL, Bilinear Enriched	811	314	814	1820	1170	2020
	Plane Stress	6 EL, Bilinear	-	-	1030	-	-	3510
		6 EL, Bilinear, Enriched	895	385	1080	2010	1990	3730
New PAPST	Plane Stress	6 EL, Bilinear	-	-	804	-	-	2079
		6 EL, Bilinear, Enriched	824	222	804	1854	931	2067
	Plane Stress	6 EL, Bilinear	-	-	999	-	-	3349
		6 EL, Bilinear, Enriched	899	379	1030	2022	2171	3484

J_{ssy} is calculated from the elastic K_I

J_s is calculated from the plastic K_p

J_p is the path value calculated by integration of the nodal stresses and strains

3.6 Tearing Modulus

Three separate models of a compact tension specimen were generated to verify the tearing calculation. In all cases, the material was bilinear with a yield stress of 138 KSI and a stress level of 152 KSI at 10% elongation. Young's modulus was 29,000 KSI, Poisson's ratio was .3, and a value of 890 in-lb/in^2 was used for J_{IC}. These properties roughly correspond to HY-130.

Each of the models contains a different level of sophistication. Model #1, shown in Figure 3.6-1, was 6 elements with the crack extension of 0.1 inches. Model #2, shown in Figure 3.6-2, was 18 elements with a crack extension of 0.05 inches. Model #3, shown in Figure 3.6-3, was 28 elements with a crack extension of 0.02 inches. The Model #2 improvement over Model #1 was to improve the grid in the vicinity of the crack tip. Model #3 enhanced this grid even more by providing a refined grid at the end of the crack growth region. It also refined the grid in the region of compression yielding near the back surface.

Each of the models was loaded in four increments. Displacement control was imposed on a spring in series with the specimen. Different spring stiffnesses were tried on Models #1 and #2 to approximate changes in machine compliances.

For each model and spring combination, two runs were made. The model was first run with the initial crack and then grown to the final length. Next the model was run with the full length crack. This was done to compare the stress state of the growing crack to the full length crack and to check for any numerical anomalies that may have occurred. None were seen.

The J value that was used for comparison was the path that fell entirely within the elastic region of the specimen. This value compares the best with the J integral estimate based on the applied load-load line displacement curve. At this time, it is felt that the deviation of the J-integral path values (previously reported) is a result of the smoothing technique that is used to determine the nodal stresses and strains. While the smoothing technique works acceptably for elastic strain fields, the complexity that arises from the elastic-plastic strain fields is not well represented by the smoothing functions.

Figures 3.6-4 through 3.6-8 show the J vs. load line displacement curves for the five cases reported. It can be seen that the higher refinement in Model #3 results in closer comparison between the growing and the grown crack predictions. Figure 3.6-9 shows the plastic zone comparison between them. It should be noted that the strain level near the crack tip was about 30% in both cases. This is far in excess of the assumed ultimate of 10%.

Figure 3.6-10 shows the tearing modulus values that were calculated from the five cases. The experimental curves that are used for comparison are from a paper by Joyce and Vassilaros (Reference 15). Several important differences should be noted:

1) The material has an ultimate stress of 152 KSI at 20% elongation. The finite element models used a slightly higher hardening material.

2) The material has a reported J_{IC} of 870 in-lb/in^2 while the "key curve" used to generate the T_{APPL} curve appears to have a J_{IC} of about 800 in-lb/in^2. The models all grew cracks near 890 in-lb/in^2.

3) The tearing curves are for continuously growing cracks. The models, by necessity, can only grow the cracks incrementally.

4) The model is idealized as plane stress. The specimens are finite thickness.

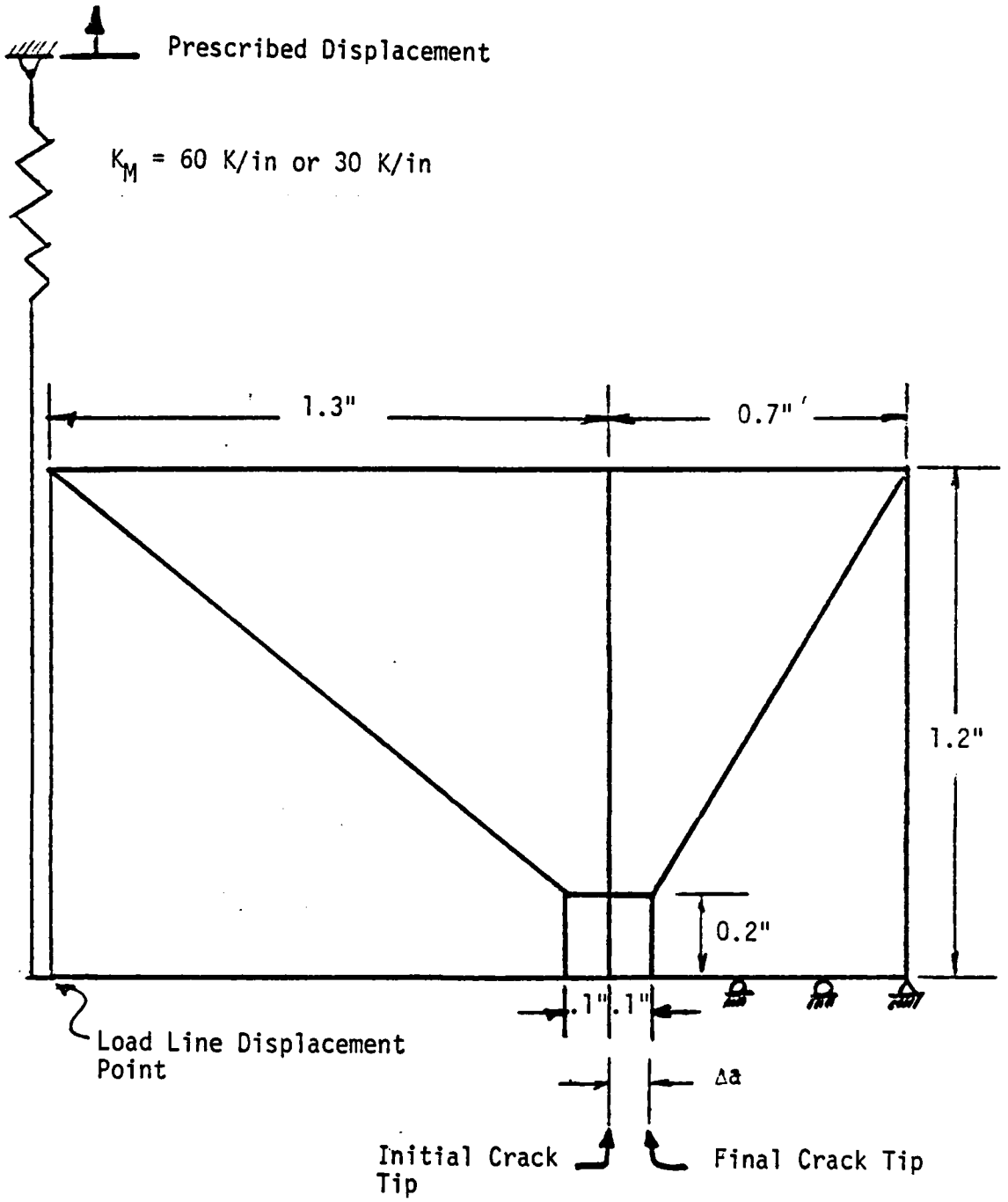

Plane Stress

$E = 29 \times 10^6$ psi

$\nu = .3$

σ_{yd} = 138 ksi

σ = 152 ksi at ε = 10%

$\beta = 1.0$

Figure 3.6-1 Model #1 - 6 Element

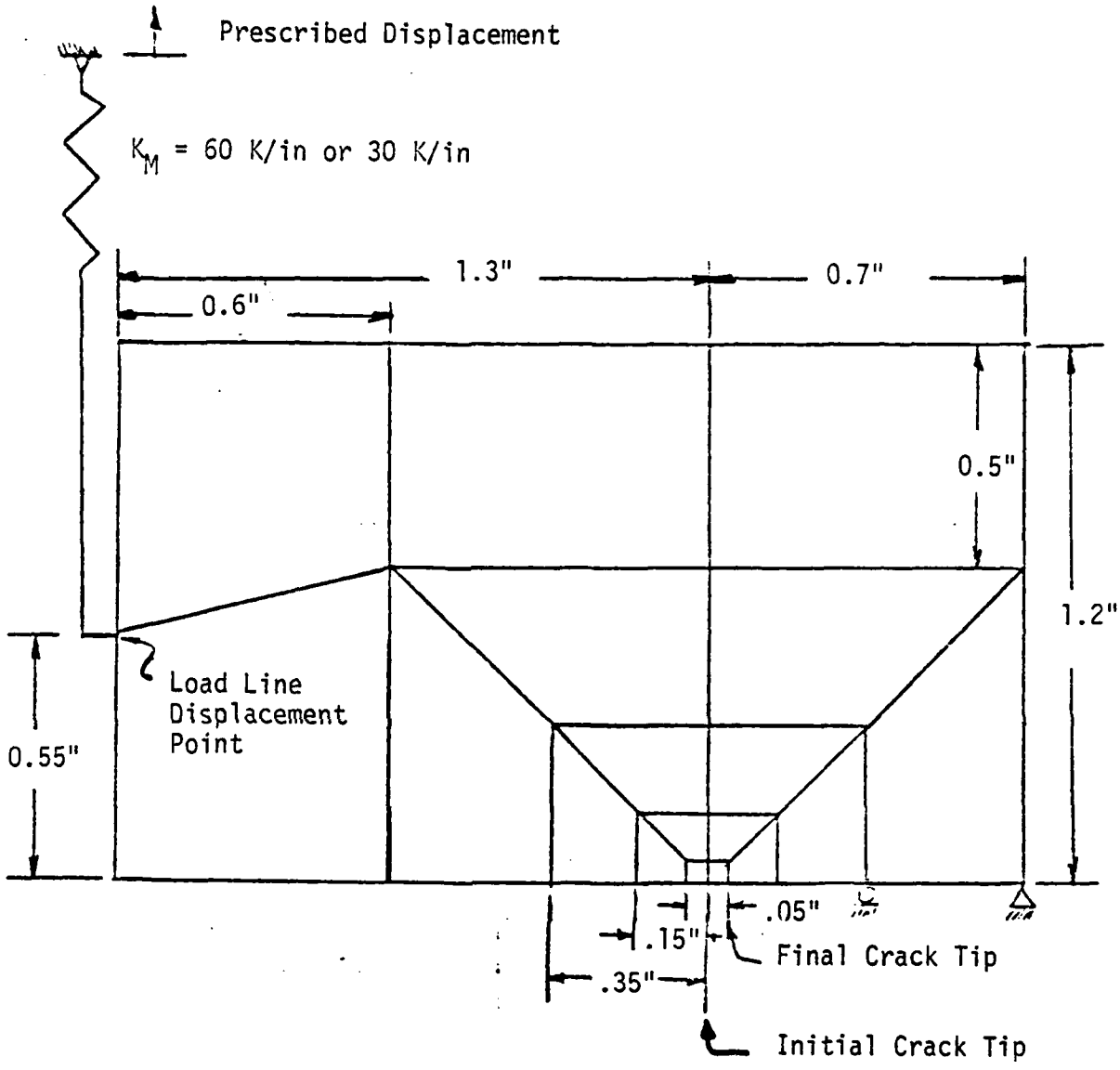

Plane Stress

$E = 29 \times 10^6$ psi

$\nu = 0.3$

$\sigma_{yd} = 138$ ksi

$\sigma = 152$ ksi at $\varepsilon = 10\%$

$\beta = 1.0$

Figure 3.6-2 Model #2 - 18 Element

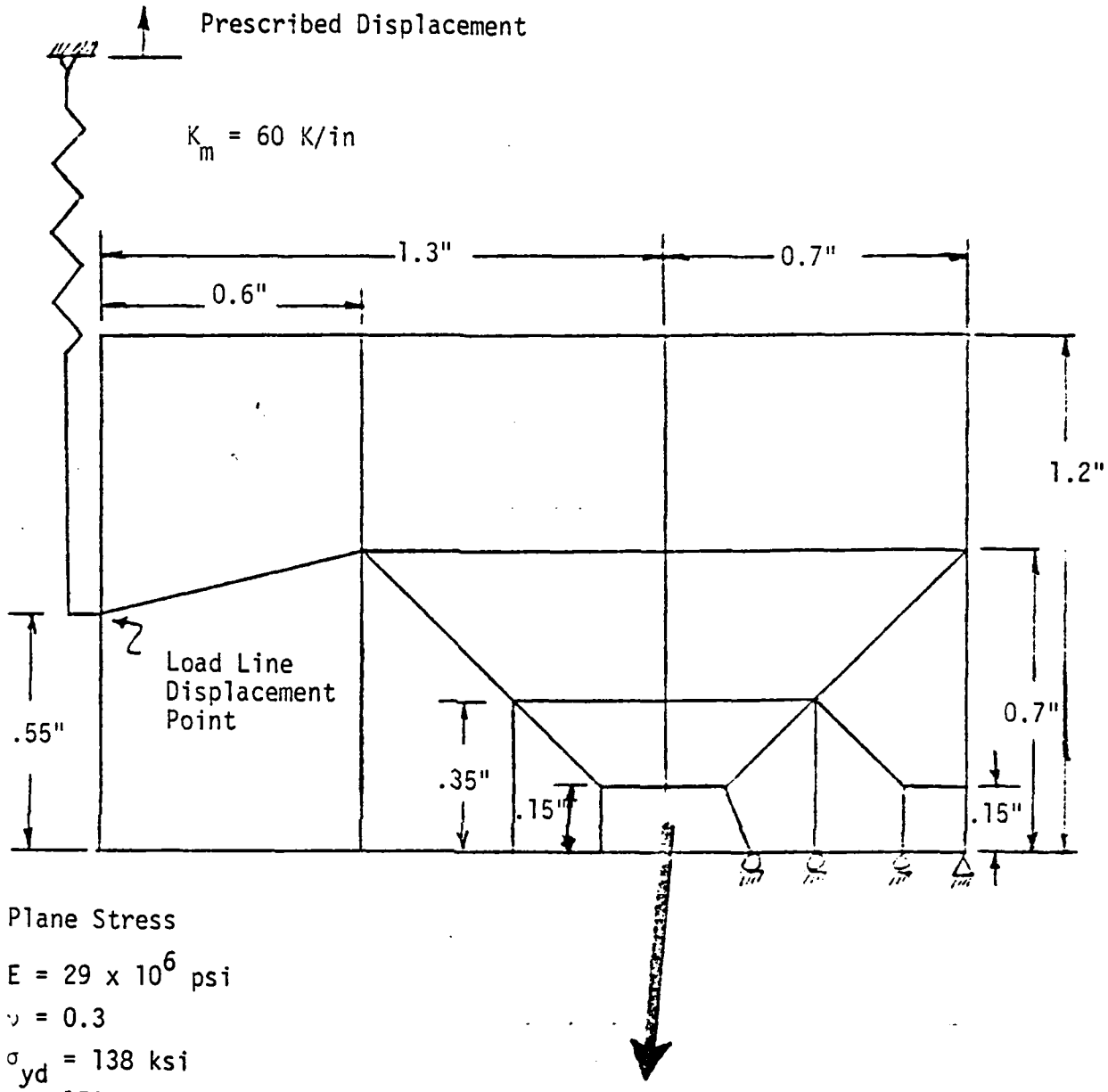

Plane Stress

$E = 29 \times 10^6$ psi

$\nu = 0.3$

σ_{yd} = 138 ksi

σ = 152 ksi at ε = 10%

$\beta = 1.0$

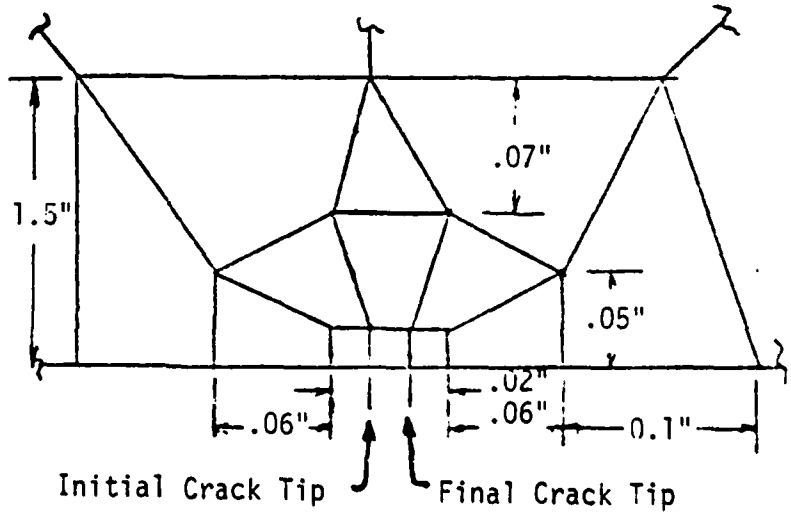

Figure 3.6-3 Model #3 - 28 Element

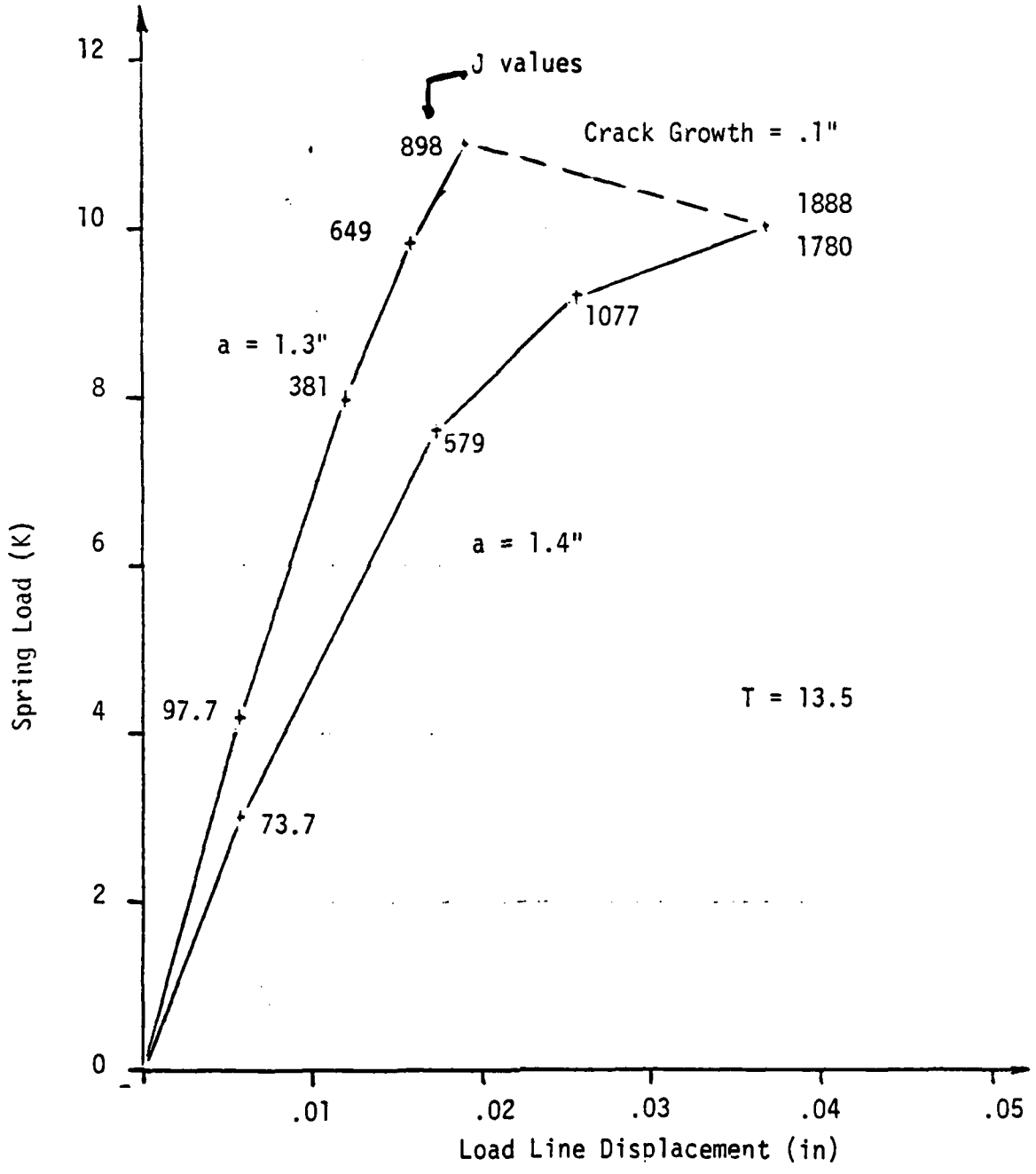

Figure 3.6-4 Model #1, J vs. Load Line Displacement, K_m = 60 K/in

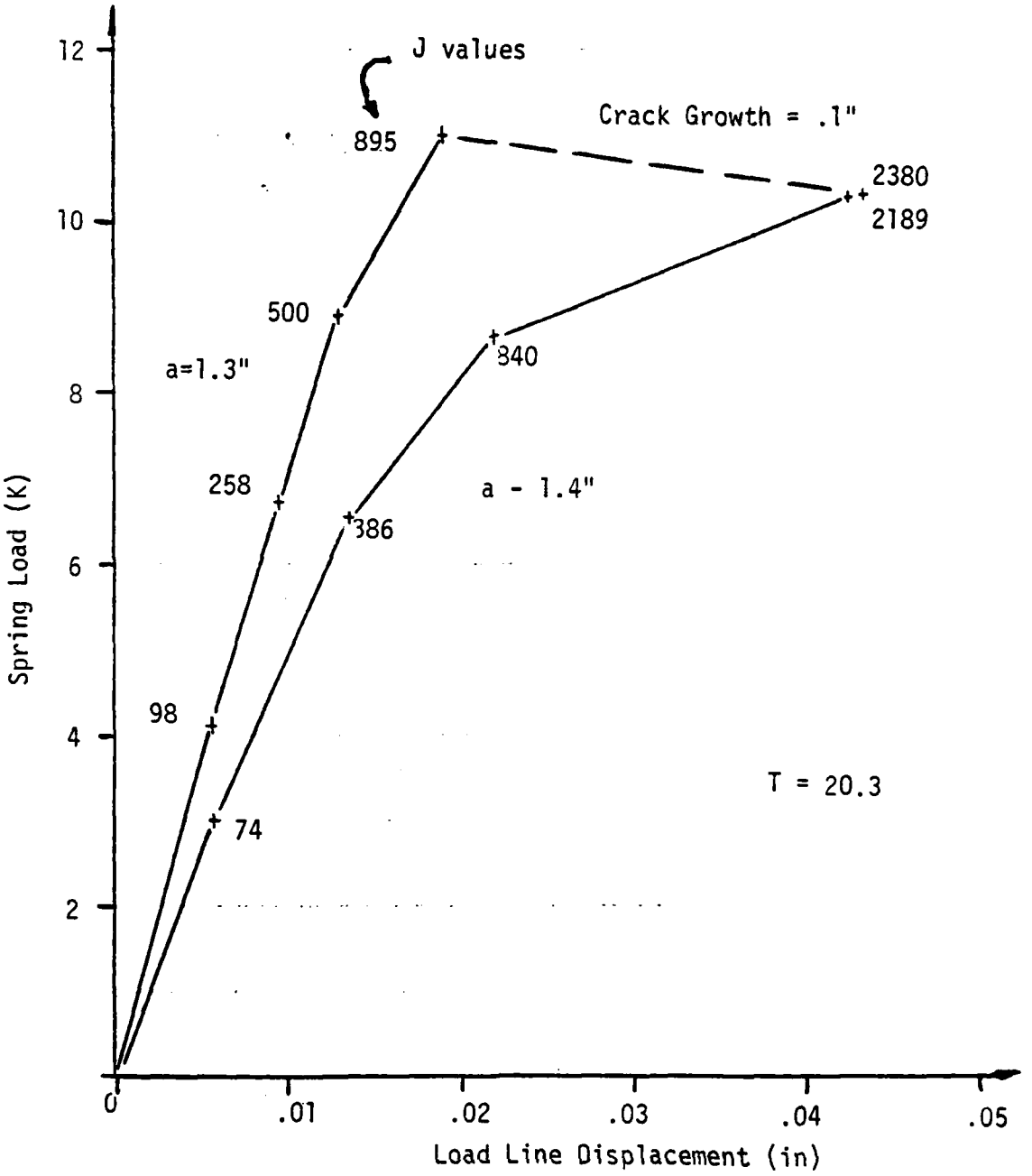

Figure 3.6-5 Model #1, J vs. Load Line Displacement, K_m = 30 K/in

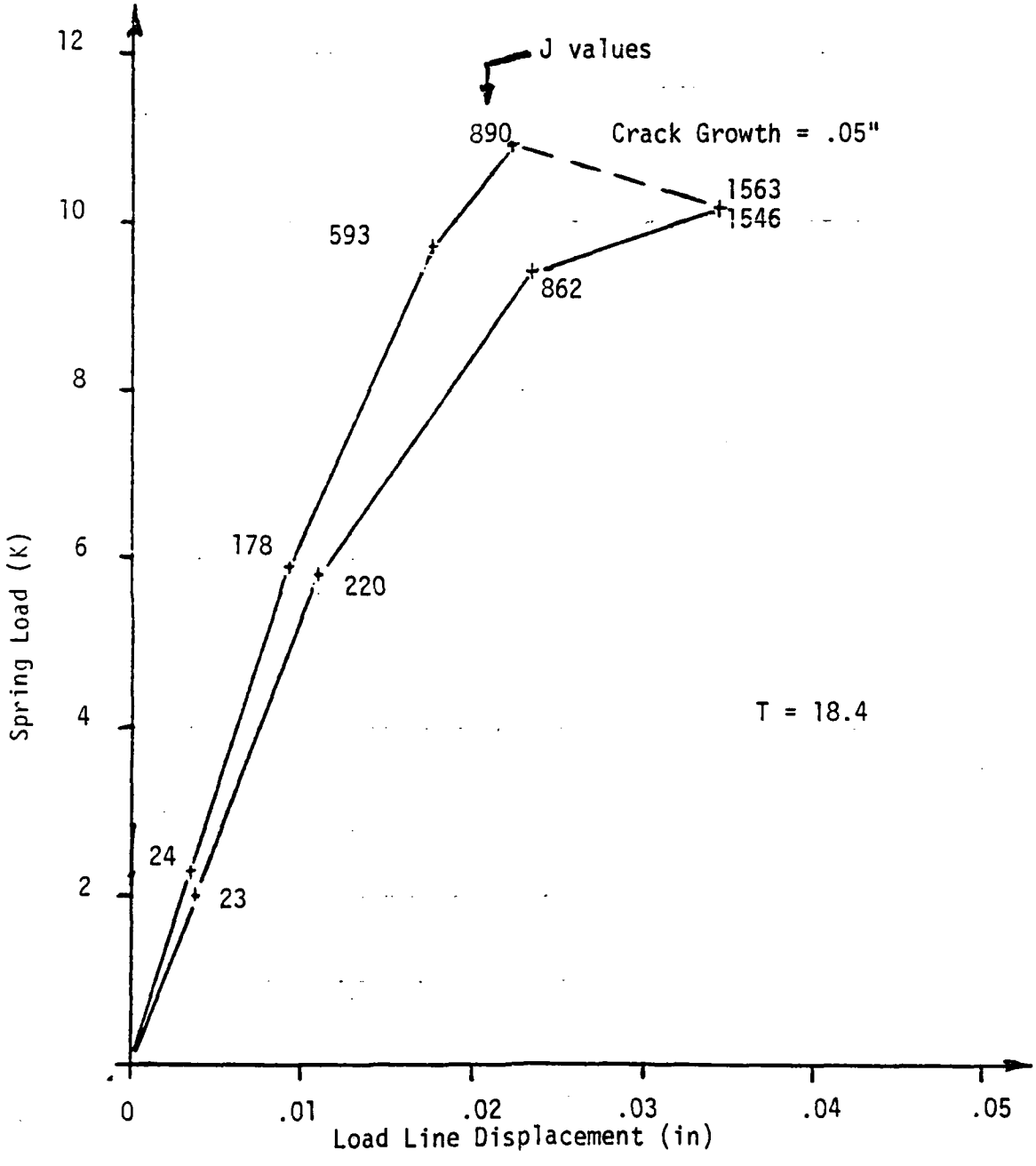

Figure 3.6-6 Model #2, J vs. Load Line Displacement, K_m = 60 K/in

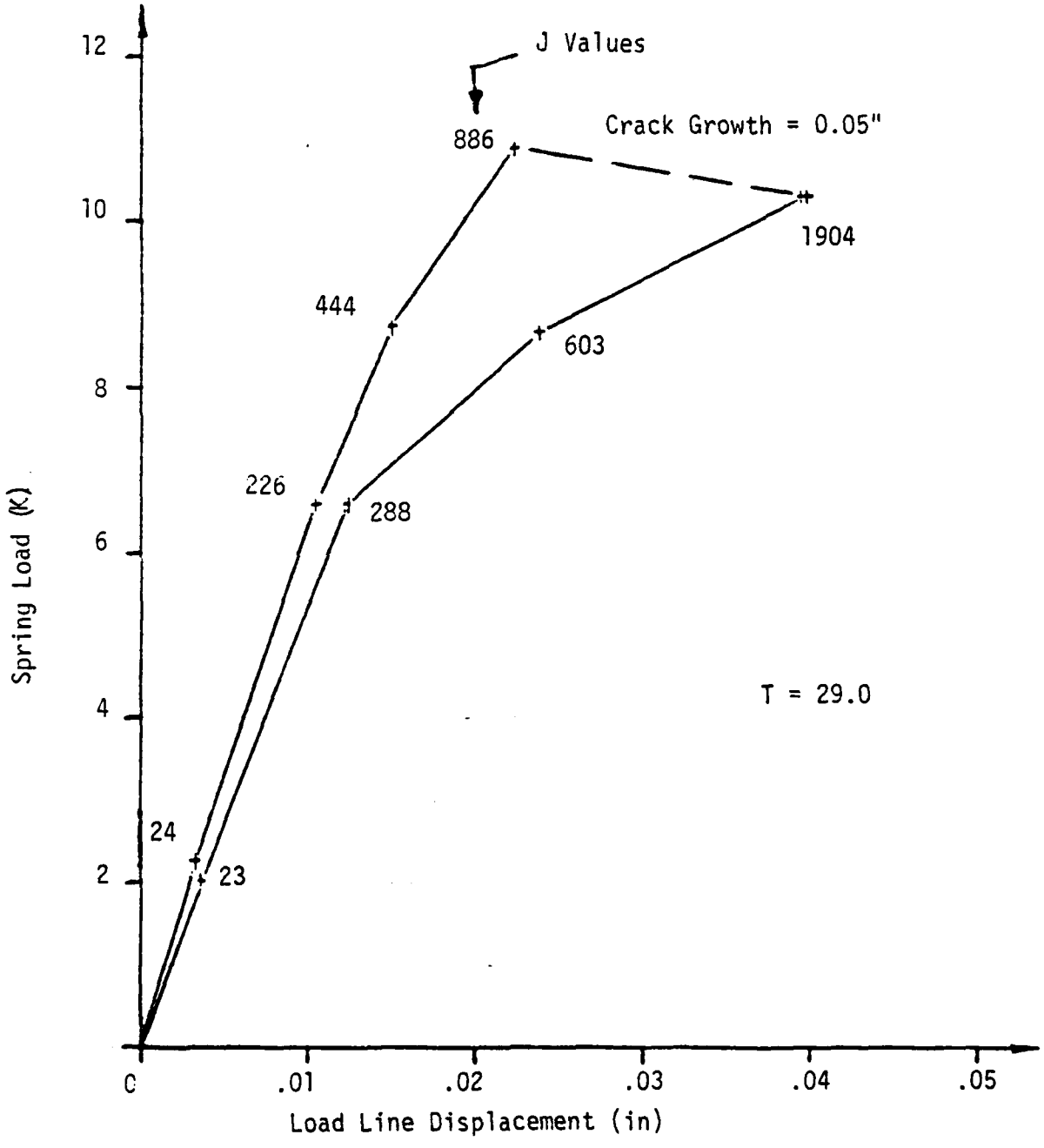

Figure 3.6-7 Model #3, J vs. Load Line Displacement, K_m = 30 K/in

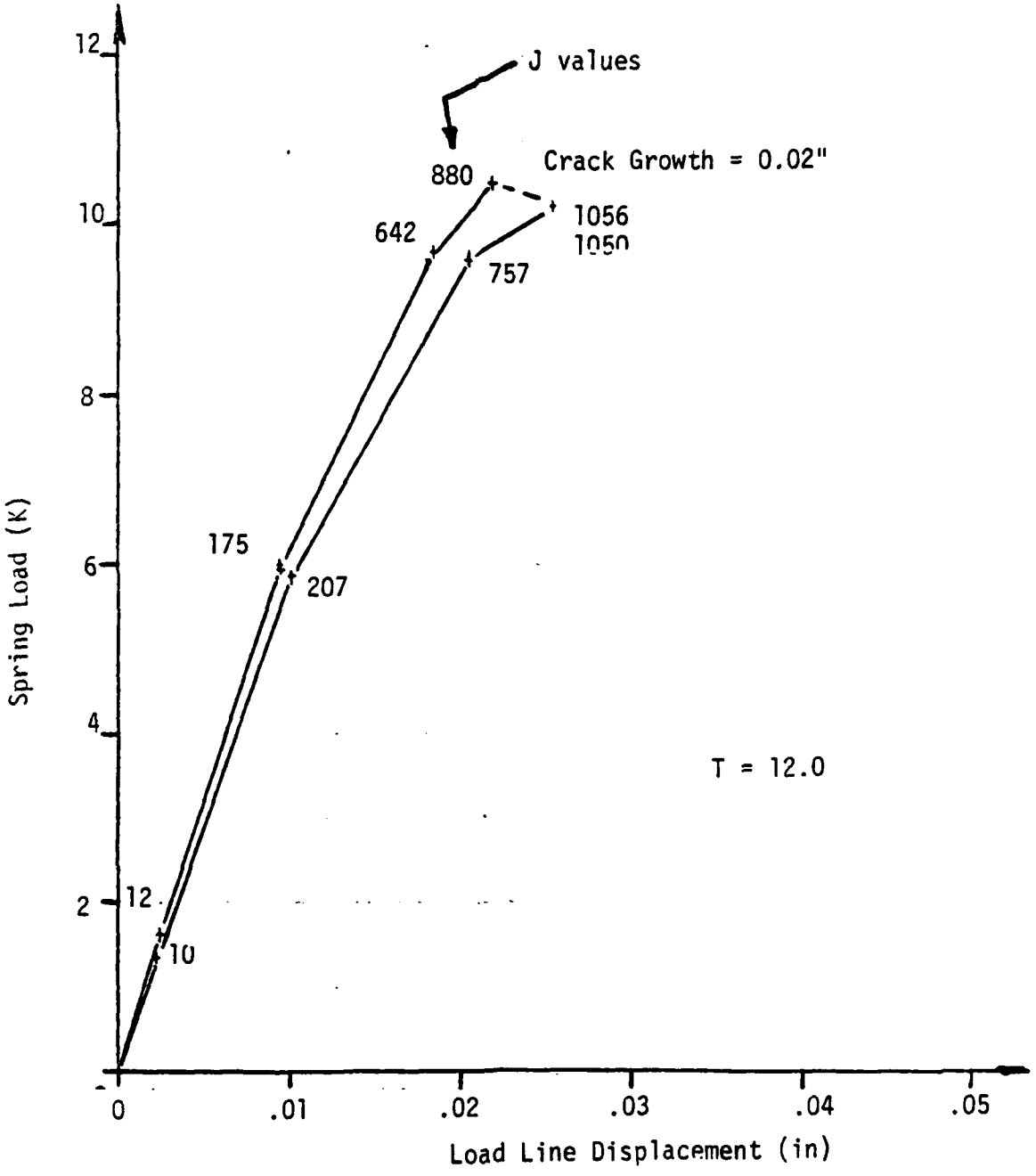

Figure 3.6-8 Model #3, J vs. Load Line Displacement, K_m = 60 K/in

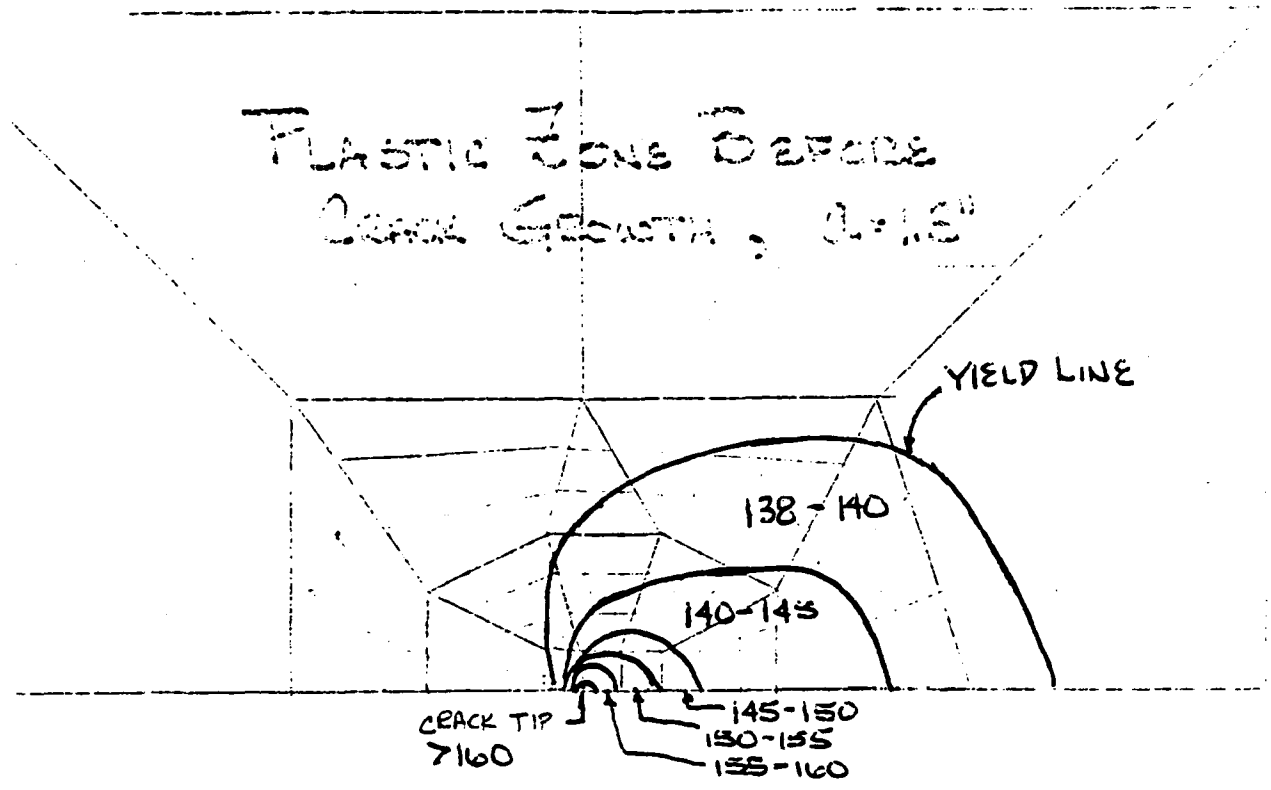

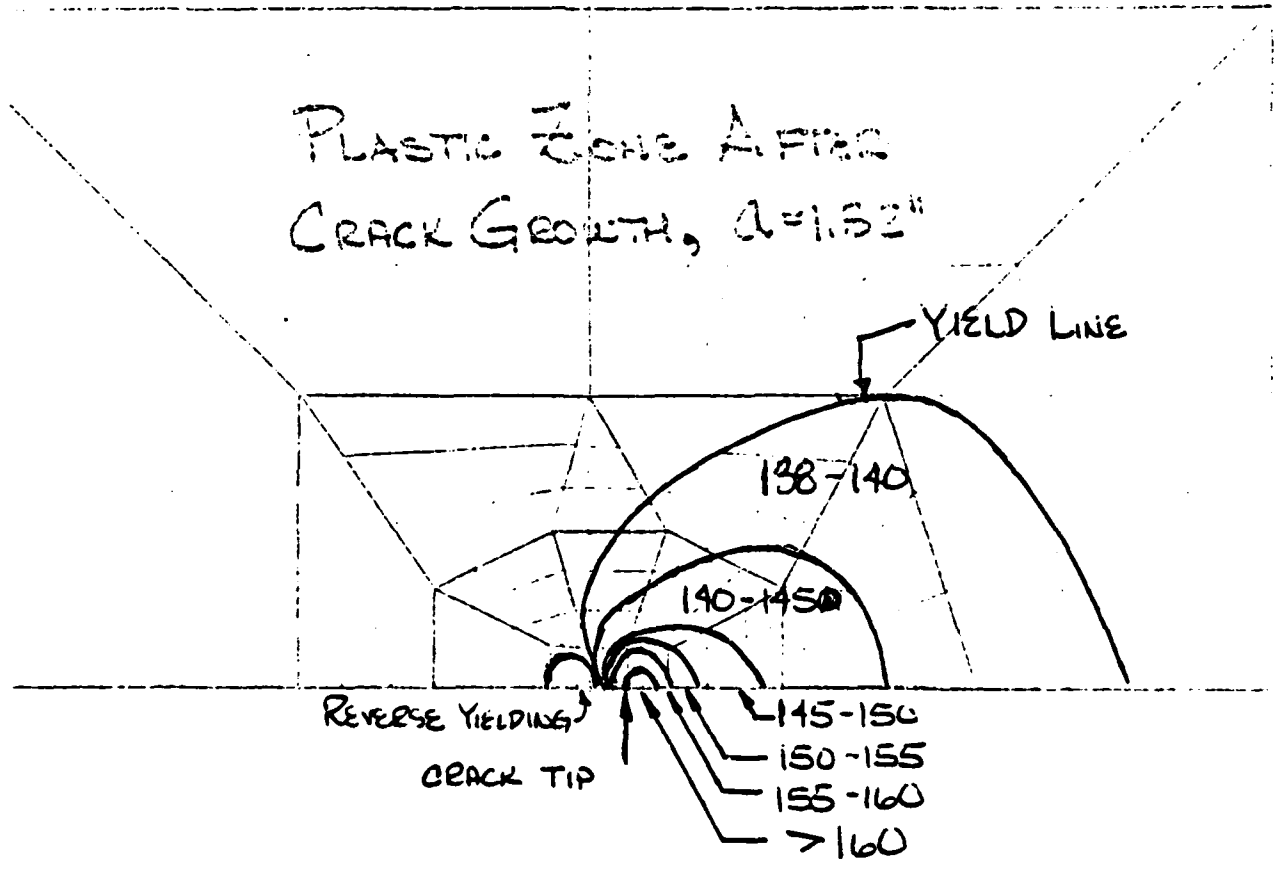

Figure 3.6-9 Plastic Zones

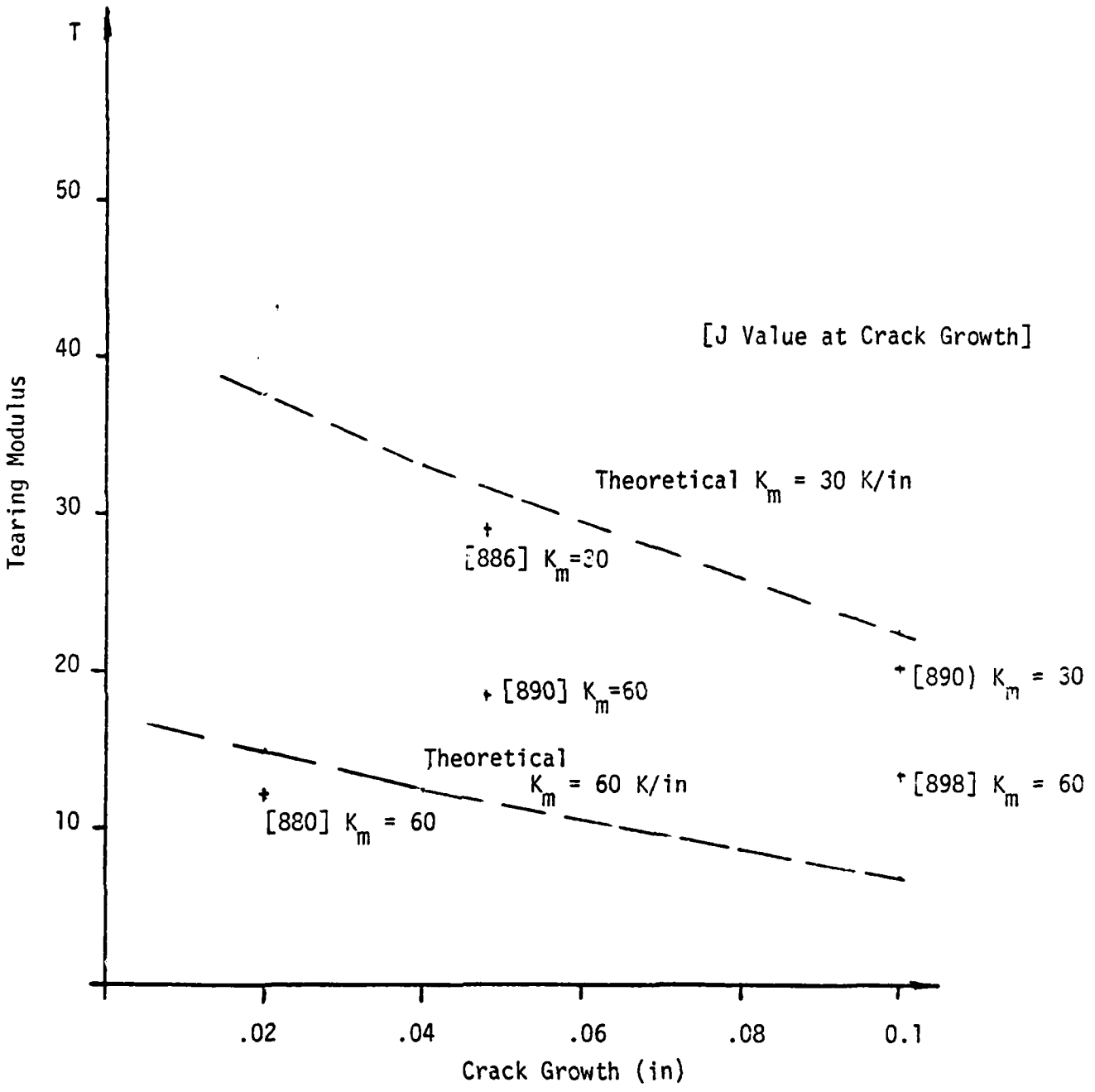

Figure 3.6-10 T_{APPL} vs Crack Extension

Theoretical Curves From Joyce & Vassilaros, STP 743, pg 539.

3.7 Thermal Loading

For verification of this coding, three separate models were each run for axisymmetry, plane strain, and plane stress:

1) Unconstrained with a uniform temperature field.

2) Constrained top and bottom with a linearly varying temperature field.

3) Constrained top and bottom with a uniform temperature field and described with bilinear elastic/plastic material properties.

Both the unconstrained and constrained models are shown in Figure 3.7-1. In all cases, the computer model matched the analytical equations.

3.7.1 Axisymmetry

Test case one, using the unconstrained model and uniform temperature, produced uniform strains and no stresses or reactions. This is the trivial theoretical case, but shows that no residual or unbalanced forces are incurred by the thermal body forces.

Test case two used the constrained model with a lineaerly increasing temperature field. This case is described generally in Reference 16. The stresses in the body are:

(3.7-1)

$$\sigma_r = \frac{\alpha E}{1-\nu}\left[\frac{1}{a^2}\int_0^a Trdr - \frac{1}{r^2}\int_0^r Trdr\right]$$

$$\sigma_\theta \quad \frac{\alpha E}{1-\nu}\left[-T + \frac{1}{a^2}\int_0^a Trdr + \frac{1}{r^2}\int_0^r Trdr\right]$$

$$\sigma_z = \frac{\alpha E}{1-\nu}\left[\frac{2\nu}{a^2}\int_0^a Trdr - T\right]$$

where a = outer radius
r = a radius within the body
T = temperature field expressed as a function of r

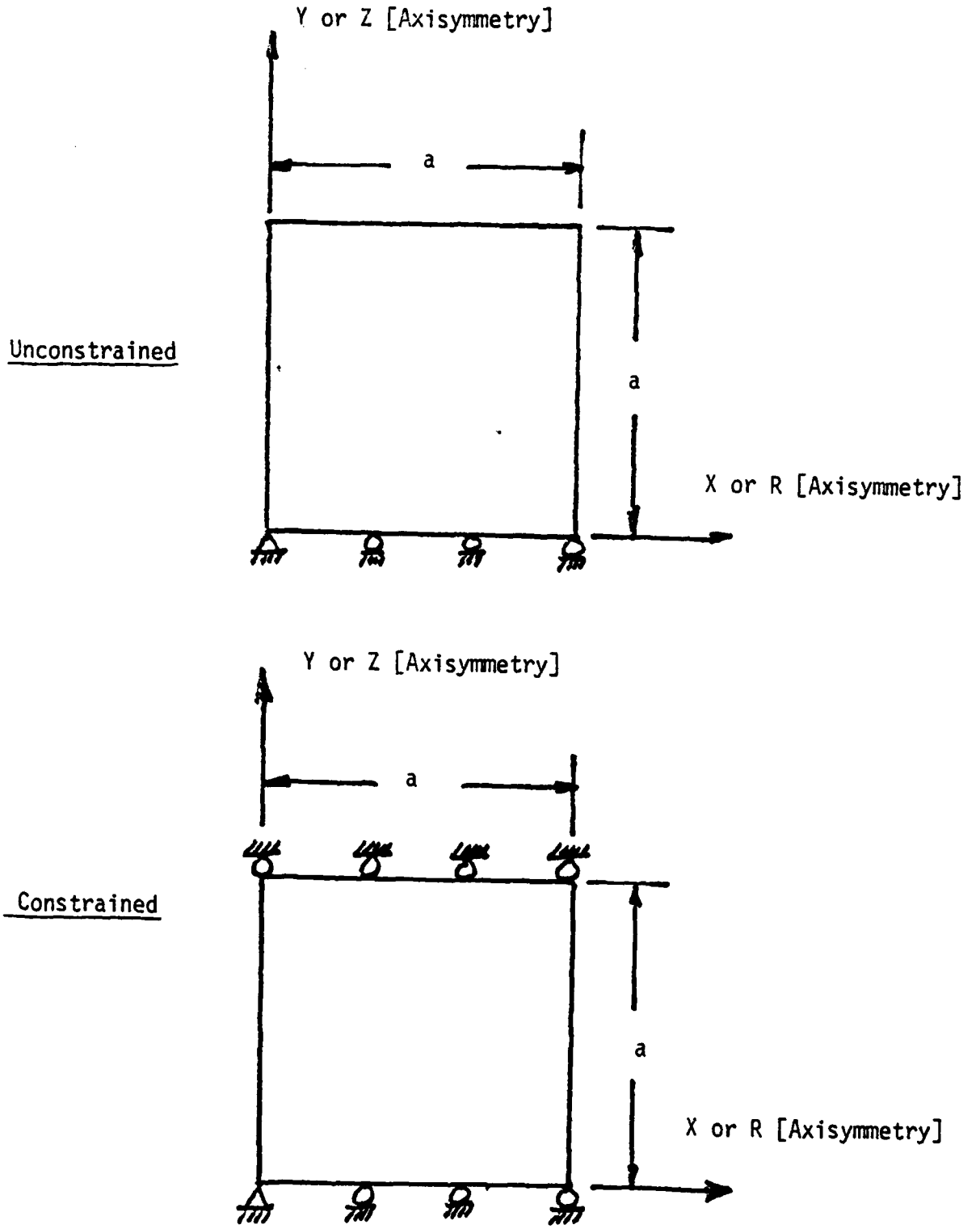

Figure 3.7-1 Thermal Models

The linear field that was used can be expressed as:

$$T = T_o \frac{r}{a} \tag{3.7-2}$$

where T_o is the temperature at r = a

Incorporating Equation 3.7-2 into 3.7-1 and integrating, we get the following stresses:

$$\sigma_r = \frac{\alpha E T_o}{3(1-\nu)} \left[1 - \frac{r}{a}\right]$$

$$\sigma_\theta = \frac{\alpha E T_o}{3(1-\nu)} \left[1 - \frac{2r}{a}\right] \tag{3.7-3}$$

$$\sigma_z = \frac{\alpha E T_o}{3(1-\nu)} \left[2\nu - \frac{3r}{a}\right]$$

We can evaluate the term in brackets at the center and at the outer radius:

	r=0	r=a
σ_r	1	0
σ_θ	1	-1
σ_z	2ν	$2\nu-3$

Test case three also used the constrained model but with a uniform temperature field. The elastic stresses in this case become:

$$\sigma_r = 0 \tag{3.7-4}$$

$$\sigma_\theta = 0$$

$$\sigma_z = -\alpha E T$$

The plastic response was described using a bilinear material model, (n = 1). The stress beyond yield in this case becomes:

$$\sigma_z = -\alpha E T_1 - \alpha \frac{E}{(1+\alpha_m)} \Delta T \qquad (3.7\text{-}5)$$

where:

α_m = slope of the stress/strain curve beyond yield

T_1 = tempereature at yield

ΔT = temperature increment beyond yield

This behavior was verified in the computer model.

3.7.2 Plane Stress

Plane stress is quite similar to axisymmetry in terms of the stress fields for this analysis. Test case one, unconstrained with uniform temperature, produces uniform expansion with zero stress. Test case three with the same material properties results in uniaxial stress of the form:

$$\sigma_y = -\alpha E T_1 - \alpha \frac{E}{1+\alpha_m} \Delta T \tag{3.7-6}$$

Test case two shows different behavior. We can treat the case of a constrained element with a linearly increasing temperature field as unconstrained expansion with a linearly increasing imposed displacement. This displacement can be described as:

$$v(x) = -\alpha a T(x) = -\alpha T_0 X \tag{3.7-7}$$

The total strains therefore are:

$$\varepsilon_y = v(x)/a + \alpha T(x) = 0 \tag{3.7-8}$$

$$\varepsilon_x = -\nu(v(x)/a) + \alpha T(x) = (1+\nu)\alpha T_0 X$$

$$\varepsilon_z = -\nu(v(x)/a) + \alpha T(x) = (1+\nu)\alpha T_0 X$$

The stress field becomes therefore:

$$\sigma_x = \sigma_z = 0 \tag{3.7-9}$$

$$\sigma_y = -\alpha E T(x) = -\alpha E T_0 X$$

3.7.3 Plane Strain

Plane strain does not have a trivial test case as do axisymmetry and plane stress. The Z direction is always constrained and stresses are produced in that direction for any thermal loading.

Test case one produces the following total strains and mechanical stresses:

$$\begin{aligned} \varepsilon_x &= (1+\nu)\alpha T_0 \\ \varepsilon_y &= (1+\nu)\alpha T_0 \\ \varepsilon_z &= 0 \\ \sigma_x &= 0 \\ \sigma_y &= 0 \\ \sigma_z &= -\alpha E T_0 \end{aligned} \tag{3.7-10}$$

Test case two can be analyzed similarly to plane stress, except that both Y and Z directions are constrained. The mechanical displacements required to offset the thermal expansion can be described as:

$$\begin{aligned} v(x) &= -\alpha a T(x) \\ w(x) &= -\alpha t T(x) \end{aligned} \tag{3.7-11}$$

where a and t are the in-plane and transverse dimensions of the plate, respectively.

The only non-zero strain is in the x direction.

$$\varepsilon_x = \frac{2\nu}{1-\nu}\alpha T(x) + \alpha T(x) = \frac{1+\nu}{1-\nu}\alpha T(x) \tag{3.7-12}$$

The resulting stress state is:

$$\begin{aligned} \sigma_x &= 0 \\ \sigma_y &= -\alpha E T(x)/(1-\nu) \\ \sigma_z &= -\alpha E T(x)/(1-\nu) \end{aligned} \tag{3.7-13}$$

When these are evaluated for the linear temperature distribution in Equation 3.7-2, they check with the results of the computer model.

Test case three results in the same strain field as described in Equation 3.7-12 except that the temperature field is constant rather than linear. The stresses become in this case:

$$\sigma_y, \sigma_z = -\frac{\alpha}{1-\nu} \left[E T_1 + \left(\frac{E}{1+\alpha_m} \right) \Delta T \right] \qquad (3.7\text{-}14)$$

where the notation is similar to Equation 3.7-5.

APPENDIX A - CHANGES IN THE INPUT FILE FOR PAPST

1) Crack Growth -

Group VIII - Nonlinear Analysis Data
C. J-Integral Related Data
Card 3 - Needed only if NCNR of card 1 is now zero.

The change in the crack growth mechanism required a modification to the user input. Only one increment of crack growth is allowed. The procedure is described in Section 2.6.3.

CARD 3 - NCN1, NCN2, NCN, JIC, SIGMAØ

FORMAT (3I5, 2F1Ø.2)

(1-5) NCN1 - Present crack tip node
(5-1Ø) NCN2 - Ultimate crack tip node
(1Ø-15) NCN - Number of iterations to release spring (5 should be adequate)
(16-25) JIC - Average value of the J-integral paths at which crack is to be grown (Note: Crack will not grow unless JIC is exceeded)
(26-35) SIGMAØ - Flow stress in Tearing Modulus Equation (2.6.3-1)

2) Elastic Analysis -

Group VIII - Nonlinear Analysis Data
A. Nonlinear Analysis Control
Card 1

If this card is left blank or NINC = 1, the program will default to an APES run (no further data required). The user is suggested to try his model in this mode before attempting a PAPST run. Cost for an elastic run may be one to two orders of magnitude less expensive.

3) Wavefront Reordering - This is so the user can change element ordering after the fact, (i.e., "grid too big for program") without changing input model data.

Automatic resequencing of the elements by the program is still in development. However, the user may manually define a resequencing. This is particularly useful if there are a large number of spring elements since they are generated at the end of the area element list. To use this facility:

Group I - Preliminary Data

Card 2:

(66-7Ø) IWAVE - option for wavefront reordering
= Ø no change (default)
= 1 user specified sequence

Group VII - Additional Data
D. Wavefront Reordering

CARDS: IN (I)
FORMAT (16I5)
TERMINATE WITH A FULLY BLANK CARD

IN(I) are lists of element numbers that refer to the position of the element in the input stream. Springs are added on at the end of the area element input and are numbered in order of appearance in input. The initial value (and default) of this list is reflected in the output in the nodal indices section.

The user may specify as many (up to 16) elements on a card as he wishes. The solution procedure will be modified internally to use the specified list. There is no effect on the output sequencing.

Unspecified elements in the list will be added, in order, to the end of the user specified list.

This solution may be preferred over modification of the element order if the user gets, or suspects to get, the error message: "GRID TOO LARGE FOR PROGRAM"

4) Convergence Criteria

Group VIII - Nonlinear Analysis Data
Card 1 C1,C2

The equations for convergence criteria have been slightly modified, see Section 2.0.3. As a result, the default values were modified. In the new code, C1 defaults 10^{-2} and C2 defaults to 10^{-4}.

APPENDIX B - NOTES ON APES AND PAPST CODES

This manual documents the current approaches and algorithms contained in PAPST. During the course of this work several areas of concern with respect to the previous versions of APES and PAPST appeared. A few coding errors in both APES and PAPST were found. Some portions of the codes were found to have questions on interpretation. Many improvements to the code were made for consistency and clarity. This Appendix addresses these areas.

Topics

1) Errors - APES
2) Errors - PAPST
3) Warnings on Interpretation - Previous Codes
4) Improvements - PAPST
5) Limitations of the new PAPST

1) Errors - APES

a) Variable NOPT or ISTRN

This variable changes value several times in the program. The subroutine BB was generated from one section of the program and is called from another where the designation has changed. It is used four times in the subroutine. In order, the changes are:

NOPT.GE.2	becomes	NOPT.LE.1
NOPT.EQ.2	becomes	NOPT.EQ.1
(x2)NOPT.NE.3	becomes	NOPT.NE.Ø

There may be other subroutines where a similar problem occurs, so the user may wish to review all references to this variable.

b) Subroutine FRON1

In the coding for inclined or rotated nodes, there is an error in the sin/cos components:

SINA*COSA becomes SINA*COSB

These changes have been implemented in the versioon of APES at DTNSRDC

2) Errors - PAPST

a) Subroutine B1 - variable interchange

In the determination of the enriching functions, the definitions of two of the variables were interchanged. The code should read:

```
TEMP8 = TEMP8 + DNF(2,I)*UX1(I)

TEMP9 = TEMP9 + DNF(1,I)*UY1(I)
```

For enriched, large displacement problems, this error has an effect on

the results.

b) Thermal Strains - DSTR

In plane strain, the thermal strains depend on the current material property matrix. This was not properly handled. See Section 2.5.4 for the correct equations. Since the material matrix is formulated differently here than in the latest program, no simple fix is described. These errors have been corrected in the latest version of PAPST available at DTNSRDC.

3) Warnings on Interpretation - Previous Codes

This section covers areas where the user may have a misunderstanding about what the program is doing. This misunderstanding may have an impact on how the user interprets his results.

a) Subroutine ENSTR-APES

This subroutine calculates the crack tip loading for crack face pressure. We have been unable to reconstruct the coding in this section. However, we have no evidence that it is wrong. The user may want to compare the crack tip contribution in the present subroutine PRESS to that in ENSTR.

b) Jaumann Stress Rate and Enriched Elements - PAPST

The rotation components used in the computation of the stress rate correction term were not updated for the enriched contributions. This will effect the answers slightly and are now included in the new program.

c) Hydrostatic Expansion - PAPST

We have found in reviewing output for the previous version of PAPST that in plastic zones, the hydrostatic stress and strain do not satisfy the equation:

$$(\sigma_{xx} + \sigma_{yy} + \sigma_{zz}) = \frac{E}{(1-2\nu)} (\varepsilon_{xx} + \varepsilon_{yy} + \varepsilon_{zz}) \qquad \text{(B-1)}$$

This is believed to be a numerical inaccuracy inherent in the former code and is satisfied in the current code.

d) Subroutine OUTPUT - Effective Stress - PAPST

The average effective stress output is the average of the effective stresses. It is not the effective stress of the averaged stresses printed on the same line. This may be confusing to the user who is trying to use the averaged stresses in conjunction with the effective stress (see Section 4 d).

e) J-Integral Path Values - PAPST

The path taken for the J-integral is taken within an element at the edge. The element is selected by sorting through the nodal indices. Rearrangement of the indices can result in a change in the elements chosen for a given path, and as a result, in a numerically different J-integral value (see Section 4 f).

4) Improvements - PAPST

a) Subroutine PRESS

This subroutine was changed from an edge integral to a line integral, simplifying the code. The crack tip loading term has been generalized to handle plastic as well as elastic singularities.

b) Deformation Gradient Contributions

The deformation derivatives (U, y and V, x) are now smoothed to the nodes in the same manner as the strain components. The enriched terms have been included in the quadrature point calculations, so that the Jaumann Stress Rate is calculated consistently.

c) Yield Surface Modification

The yield surface is updated only for converged increments. The scaling algorithm for increments crossing the yield surface has been substantitally revised. This seems to reduce the problem of yield surface "wandering" during iterations. Equation B-1 also seems to be enforced more accurately.

d) Subroutine OUTPT2 - Effective Stress

The effective stress listed with the averaged and principle stresses is calculated from the averaged stresses. This keeps the output self-consistent.

e) Stress Intensities

The stress intensity coding has been completely redone. The elastic and plastic singularities now use forms of the same equations.

f) J-Integral, Path Values

The J-Integral has been rewritten so that it uses the averaged nodal stress and strain values. This removes any sequencing dependence and appears to give more consistent results.

g) Thermo-Plasticity

The thermo-plastic analysis has been re-written to fully incorporate all of the plasticity effects.

5) Limitations of the New PAPST

a) Smoothing Functions

Comparison of nearby quadrature point stress levels with the smoothed nodal values has brought up a question of adequacy of the smoothing functions in regions of high plasticity. It is felt that some of the divergence of the J-integral path values may be a result of this limitation.

b) Orthotropic Plasticity

The program is designed to do orthotropic elasticity or isotropic plasticity. While the program will accept orthotropic values for a plasticity problem, the user is warned against doing this. The program may or may not run if the user does specify these types of parameters. The validity of the results, if any, could only be determined by the user. We have not tested this case as it constitutes an incorrect application of the program.

Appendix C - JCL and Usage

Version 2.0 of PAPST has been broken into two separate programs. SPAPST is the source code for the analysis program. SPPOST is the source code for the plotting package. The following files are of interest to the user:

TAPE5 - Local name for the input file
TAPE6 - Local name for the output file
TAPE47 - Binary file passed between PAPST and PPOST with information for plotting
TAPE48 - Plotting file from PPOST to be passed to plotting hardware

Table C.1 gives an example of how a typical job control file (JCL) might be set up for a CDC machine.

TABLE C.1

Example JCL Run File

```
JCL                          COMMENTS
---                          --------

/JOB
/USER
/CHARGE
GET,TAPE5=IFN.               IFN=INPUT FILE NAME
REWIND,TAPE5.
GET,PAPSTB.                  PAPSTB=BINARY CODE FOR PAPST
PAPSTB.                      EXECUTE PAPST.
COTO,1DONE.
EXIT.
1DONE.*.
REWIND,TAPE6.
REPLACE,TAPE6=OFN.           OFN=OUTPUT FILE NAME.
REWIND,TAPE47.               (IF TAPE47 DOESN'T EXIST, DROP TO EXIT.)
GET,PPOSTB.                  PPOSTB=BIANRY FOR PPOST.
PPOSTB.                      EXECUTE PPOSTB.
REWIND,TAPE48.
REPLACE,TAPE48=PFN.          PFN=PLOT FILE NAME.
GOT,2DONE.
EXIT.
2DONE.*.
DAYFILE,DFN.                 DFN=DAYFILE NAME.
REPLACE,DFN.
/EOR
```

END

FILMED

10-85

DTIC